



HAL
open science

Aptian – Early Albian Sedimentation In The Essaouira-Agadir Basin, Western Morocco

Walid Hassanein Kassab, Khadija El Hariri, Etienne Jaillard, Walid Hassanein Kassab, Fabienne Giraud, Emmanuel Robert, Moussa Masrour, Lhoussaine Bouchaou, Khadija El Hariri, Mohamed S Hammed, et al.

► **To cite this version:**

Walid Hassanein Kassab, Khadija El Hariri, Etienne Jaillard, Walid Hassanein Kassab, Fabienne Giraud, et al.. Aptian – Early Albian Sedimentation In The Essaouira-Agadir Basin, Western Morocco. *Cretaceous Research*, 2019, 102, pp.59-80. 10.1016/j.cretres.2019.04.008 . hal-02113416

HAL Id: hal-02113416

<https://hal.science/hal-02113416v1>

Submitted on 28 Apr 2019

HAL is a multi-disciplinary open access archive for the deposit and dissemination of scientific research documents, whether they are published or not. The documents may come from teaching and research institutions in France or abroad, or from public or private research centers.

L'archive ouverte pluridisciplinaire **HAL**, est destinée au dépôt et à la diffusion de documents scientifiques de niveau recherche, publiés ou non, émanant des établissements d'enseignement et de recherche français ou étrangers, des laboratoires publics ou privés.

1 **APTIAN - LOWER ALBIAN SEDIMENTATION IN THE**
2 **ESSAOUIRA-AGADIR BASIN, WESTERN MOROCCO**

3
4 Etienne Jaillard¹, Walid Hassanein Kassab², Fabienne Giraud¹, Emmanuel Robert³, Moussa
5 Masrour⁴, Lhoussaine Bouchaou⁴, Khadija El Hariri⁵, Mohamed S. Hammed², Mohamed F.
6 Aly².

7
8 1 : Université Grenoble Alpes, ISTerre, IRD, CNRS, IFSTTAR, CS 40700, 38058 Grenoble
9 Cedex 9, France. Etienne.Jaillard@univ-Grenoble-Alpes.fr

10 2 : Earth Science Department, Cairo University, Gizah, Egypt.

11 3 : Université Lyon 1, ENS Lyon, CNRS, UMR 5276 LGLTPE, 69622 Villeurbanne, France.

12 4 : Université Ibn Zohr, Faculté des Sciences, Département de Géologie, Laboratoire LAGAGE,
13 BP 8106, Cité Dakhla, Agadir, Morocco.

14 5 : Université Cadi Ayyad, Faculté des Sciences et Techniques-Guéliz, Département Sciences
15 de la Terre, Avenue Abdelkrim el Khattabi, BP 549, 40000 Marrakech, Morocco.

16
17
18 **ABSTRACT**

19 Aptian to early Albian times are marked by various geodynamic and paleoenvironmental events such as
20 large igneous province volcanism , perturbations of climate and the carbon cycle, and sea-level changes.
21 The Essaouira-Agadir basin (EAB), located on the Atlantic passive margin of Morocco, offers good and
22 fossiliferous exposures of the Aptian-Albian sedimentary series. A detailed analysis of this succession
23 made it possible to establish a biostratigraphic framework. The identification of discontinuities allowed
24 to define eight depositional sequences. As most of them are correlatable with depositional sequences of
25 other Tethyan areas, they suggest that eustacy was the main parameter controlling sedimentation. The
26 analysis of sedimentary facies and nannofossil assemblages provides information on
27 paleoenvironmental changes.

28 Sedimentation in the EAB evolved from a very low energy, carbonate ramp in the early Aptian to a low
29 energy, slightly deeper, mixed carbonate-clastic ramp in the early Albian. This change occurred along
30 with an increase of clastic input, a change from oligotrophic to mesotrophic faunal assemblages, and a
31 decrease of sea-surface temperatures. The occurrence of current sedimentary features, sporadic
32 dysaerobic deposits and local phosphatic and glauconitic crusts suggests that upwelling currents were
33 significant during this period.

34 Paleogeographic and isopach maps support a transgressive trend in the late Aptian and early Albian, and
35 unravel subsidence anomalies suggesting mild halokinetic movements during Aptian–early Albian times.

36
37 **Keywords:** Early Cretaceous, sedimentology, sequence stratigraphy, paleoenvironment,
38 paleogeography

39
40 **I. INTRODUCTION**

41 The Aptian to early Albian time is a period of important oceanographic, climatic and
42 geodynamic changes. In fact, this period recorded the earliest significant Oceanic Anoxic Event
43 (OAE) of the Cretaceous crises in the biological and/or carbon cycles, resulting in deposition
44 of organic-rich “black shales” (e.g. Schlanger and Jenkyns, 1976; Giorgioni et al., 2015). The
45 rifting and opening of the Atlantic ocean at equatorial latitudes (e.g. Moulin et al., 2010;
46 Klingelhofer et al., 2016) opened new N-S oceanic connections, whereas the former Tethyan

47 system was dominated by E-W oceanic circulations. A warm climate, related to the greenhouse
48 effect (Föllmi, 2012) was followed by significant cooling of the global ocean and climate in the
49 late Aptian (Bottini et al., 2015). The emplacement of large igneous provinces influenced global
50 climate (Kuroda et al., 2011). Noticeable, widespread lower Aptian carbonate shelves
51 developed during the early Aptian (e.g. Skelton and Gili, 2012), and a significant sea-level fall
52 in the early Aptian was followed by a marked late Aptian–early Albian sea-level rise recorded
53 in most areas around the world (Haq, 2014). Therefore, Aptian–early Albian times have been
54 extensively studied in the North-Tethyan margin, but remain relatively poorly studied
55 elsewhere. The sedimentary record of Aptian-early Albian is poorly known in northern Africa,
56 likely because it consists either of carbonate shelf, or of sand-rich deposits poor in ammonites
57 (e.g. Burollet, 1956; Vila, 1980), or of shelf marls rich in endemic ammonite fauna (e.g. Latil,
58 2011; Robert in Peybernès et al., 2013; Luber et al., 2017). The Western Atlas of Morocco
59 offers a good opportunity for studying the Aptian–early Albian period, since good exposures
60 of fossiliferous successions are easily accessible.

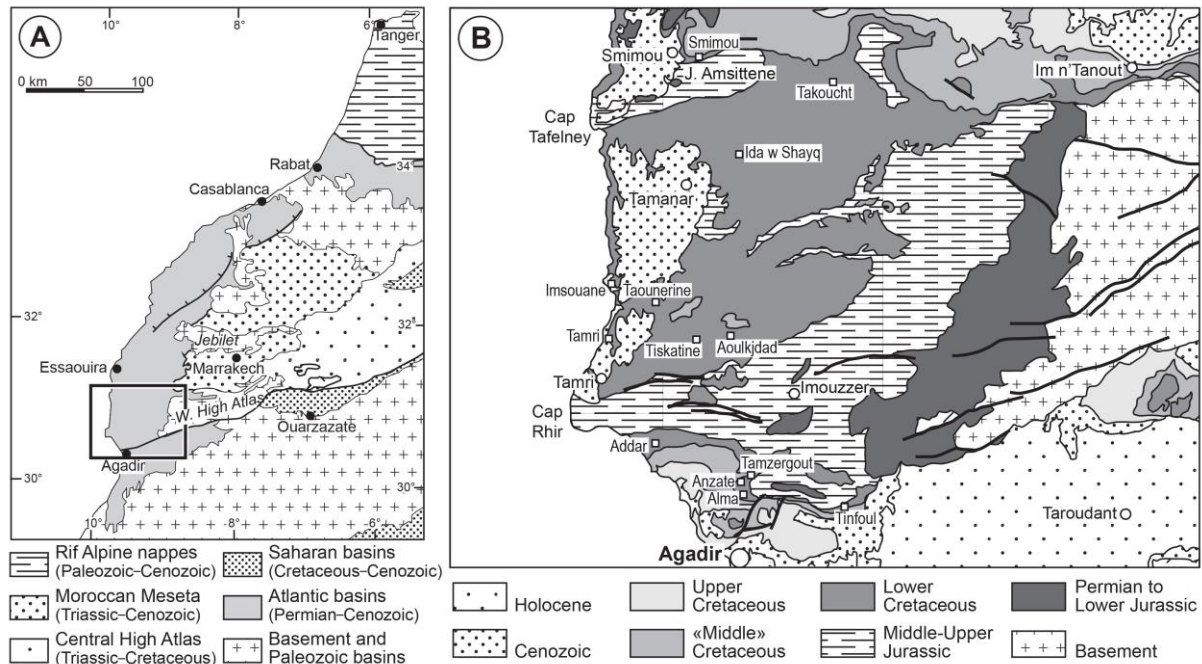
61 We did a stratigraphic and sedimentological study of the Aptian–lower Albian deposits of the
62 Essaouira-Agadir Basin (EAB), which constitutes the Western end of the Atlas chain (Fig. 1).
63 Here, we present a preliminary biostratigraphic scheme, a detailed sedimentological analysis
64 mainly based on field observations along thirteen sections distributed in the central and southern
65 parts of the EAB, a sequence stratigraphic interpretation of this succession and a
66 paleogeographic synthesis of the sedimentary evolution of the basin. In order to better constrain
67 paleoenvironments, we provide additional data on calcium carbonate content, total organic
68 carbon (TOC) and calcareous nannofossils. These data are compared to sedimentary facies to
69 better understand the temporal and spatial relationships between carbonate production, primary
70 productivity, oxygenation of the water column, and organic carbon burial during changes in
71 both sea-surface temperature and sea level.

72

73 **II. GEOLOGICAL BACKGROUND**

74 The EAB (Fig. 1) belongs to the Atlantic passive margin. Its Mesozoic sedimentary history
75 began with the Tethyan rifting, which eventually provoked the opening of the Central Atlantic
76 (Zühlke et al., 2004; Hafid et al., 2008; Schettino et al., 2009). Therefore, it has been marked
77 by strong extensional tectonics from Late Permian to early Liassic times, coeval with deposition
78 of thick red beds, overlain by shales and evaporites interbedded with basaltic flows, and sealed
79 by a pre-Pliensbachian unconformity (Hafid, 2000). An extensional regime prevailed until the
80 Late Cretaceous, and favoured the deposition of shallow marine deposits in the EAB. Shelf
81 carbonates deposition prevailed during the Jurassic and was interrupted by regressions in
82 Middle and latest Jurassic times (Stets, 1992), due to the general uplift of the High Atlas (Frizon
83 de Lamotte et al., 2008). The Early Cretaceous is marked by the deposition of thick, mainly
84 marly marine deposits, sporadically interrupted by clastic deposits deriving from the East (late
85 Hauterivian, late Barremian; Canérot et al., 1985; Rey et al., 1988; Masrour et al., 2004; Witam,
86 1998; Al Yacoubi et al., 2017). Aptian to Turonian times are represented by marine, marly and
87 calcareous strata (Ambroggi, 1963; Bourgeoini et al., 2002; Ettachfini et al., 2005; Jati et al.,
88 2010; Peybernès et al., 2013). The Upper Cretaceous mainly calcareous sedimentation (Andreu,
89 1989) was then disturbed by a first Santonian-Campanian compressional deformation (Guiraud
90 and Bosworth, 1997) and became mostly clastic (Algouti et al., 1999). The Tertiary Alpine
91 compression (mainly middle-late Eocene to Pleistocene) then inverted the Lower Jurassic
92 normal and transcurrent faults, and folded the EAB (Hafid, 2000; Frizon de Lamotte et al., 2000,
93 2008, 2011). Offshore in the EAB, salt tectonics are well documented to have been active in
94 Middle Jurassic and Late Cretaceous-Eocene times, with local activity in the Early Cretaceous
95 (Hafid, 2000; Davison et al., 2010; Tari and Jabour, 2013). Brautigam et al. (2009) and Bertotti

96 and Gouiza (2012) mentioned Upper Jurassic-Lower Cretaceous syndepositional tectonics,
 97 which they hypothetically related to compressional strain in part of the EAB.



98
 99 *Figure 1. Location of the study area. A. Location of the Essaouira-Agadir basin. B. Geological sketch*
 100 *of the EAB, and location of the studied sections.*

101
 102 The EAB is presently bounded to the North by the Jebilet High, and to the East and South by
 103 the High Atlas (Hafid, 2000) (Fig. 1). The Mesozoic sedimentary strata of the EAB dip gently
 104 towards the West. The western part of the EAB is divided into three parts by two major E-W
 105 trending anticlines, the Amsittene and Imouzzer anticlines, the western tips of which form the
 106 Cap Tafelney and the Cap Rhir, respectively (Fig. 1). Between these two major folds, a minor,
 107 smooth, E-W trending anticline separates two gentle synclines where Aptian–Albian deposits
 108 crop out (Fig. 1B). In the western part of the EAB, uplifted Pliocene marine terraces truncate,
 109 and unconformably overlie, the Mesozoic series, and are presently at 50 to 100 m above sea
 110 level.

111 Most of our present knowledge on the Aptian–Albian stratigraphy is due to Gentil (1905) and
 112 Roch (1930), who first described ammonites from this area, to Ambroggi (1963), who proposed
 113 an exhaustive stratigraphic scheme for the EAB, based on detailed lithostratigraphic
 114 descriptions and associated fossil determination, to Duffaud et al. (1966), who published a
 115 synthesis of the area and defined formations in the Cretaceous series, and to Rey et al. (1988),
 116 Witam (1998) and Bourgeoini et al. (2002), who conducted micropaleontological studies on the
 117 Lower Cretaceous succession. More recently, Peybernès et al. (2013) and Lubet et al. (2017;
 118 2019) proposed preliminary stratigraphic, sedimentological and paleoenvironmental analysis
 119 of the upper Aptian–lower Albian series of the EAB. According to these authors, the Aptian–
 120 lower Albian sedimentary rocks rest on red beds and massive sandstones of the Bouzergoun
 121 Formation (Fm) of late Barremian age, and encompasses (i) the Tamzergout Fm, made of
 122 marlstone and limestone of early Aptian age, (ii) the alternating marlstone and limestone of the
 123 Tadhart Fm of early late Aptian age, (iii) the thin, marly Lemgo Fm of latest Aptian age, and
 124 (iv) the mainly marly Oued Tidzi Fm, of early to late Albian age (Fig. 2).

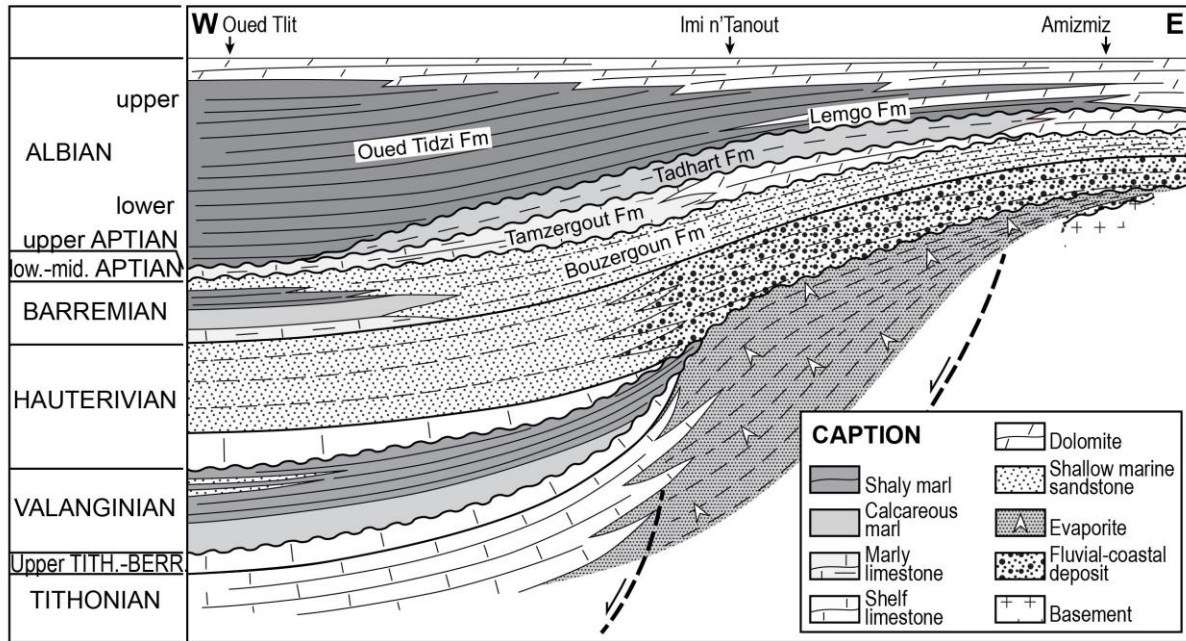


Figure 2. The Lower Cretaceous deposits in the northern part of the Essaouira-Agadir basin, part of the Atlantic passive margin, from Rey et al. (1988), modified.

In this work, we shall use the biostratigraphic scheme based on ammonites by one of us (E.R.), which has been published in Peybernès et al. (2013). The study area encompasses the area comprised between the city of Agadir, and the northern major anticline (jebel Amsittene). Thirteen sections of the Aptian–lower Albian series have been studied: five are located south of the Imouzzer anticline, five to the north of the latter, and three at the Amsittene anticline latitude (Fig. 1B, Table 1).

Section	Base	Top
Addar	30°36'04"N – 9°43'31"W	30°35'54"N – 9°43'04"W
Alma	30°31'47"N – 9°35'45"W	30°31'54"N – 9°35'46"W
Anzate	30°32'18"N – 9°35'08"W	30°32'23"N – 9°35'10"W
Aoulkjedad	30°45'47"N – 9°35'31"W	30°46'17"N – 9°35'58"W
Ida w Shayq	31°03'35"N – 9°36'04"W	31°03'31"N – 9°36'01"W
Imsouane	30°50'33"N – 9°48'54"W	
Smimou	31°11'39"N – 9°39'56"W	31°11'42"N – 9°39'56"W
Takoucht	31°09'52"N – 9°24'17"W	31°09'56"N – 9°24'37"W
Tamri	30°45'49"N – 9°48'40"W	30°45'47"N – 9°48'38"W
Tamzergout	30°32'47"N – 9°34'01"W	30°32'40"N – 9°34'12"W
Taounerine	30°48'35"N – 9°44'27"W	30°48'45"N – 9°44'19"W
Tinfoul	30°32'27"N – 9°24'53"W	30°32'24"N – 9°24'58"W
Tiskatine	30°45'43"N – 9°39'14"W	30°46'06"N – 9°39'23"W

Table 1. Geographical coordinates of the studied sections (see Fig. 1B).

III. MATERIAL AND METHOD

III.1. Sedimentology and biostratigraphy

Twelve sections have been studied in the central and southern parts of the EAB (Fig. 1B), which are 30 to 120 m thick, except for the Tamri and Imsouane condensed sections, whose

142 thicknesses do not exceed 20 m. All sections have been measured, studied and sampled bed by
143 bed for paleontological study. Most sedimentological observations have been made in the field,
144 where the lithology, sedimentary features (texture, bioturbation, current figures, dissolution or
145 erosion features etc.), mineral concentrations and faunal assemblages have been carefully noted.
146 Particular attention was paid to the lower and upper bed surfaces, as they bear important
147 information on sedimentary discontinuities.

148 When present, ammonites were extensively collected bed by bed, and precisely located along
149 the studied section. Ammonites consist of pyritic, phosphatic or calcareous molds, the latter
150 being less well preserved. After transport to France, these thousands of ammonites were cleaned
151 and studied by one of us (E.R.), through comparisons with specimens or casts preserved in
152 museum and university collections, and thanks to the large paleontological collection and
153 library available at the University of Lyon.

154 **III.2. Calcimetry and rock-eval pyrolysis**

155 The calcium carbonate content was measured in 195 samples from five sections (Takoucht, Ida
156 w Shayq, Tiskatine, Anzate and Tinfoul) and in 49 new samples from the Addar, Tamzergout
157 and Alma sections, for which previous results have been published (Peybernes et al., 2013).
158 The calcium carbonate content was determined using the carbonate bomb technique (Müller
159 and Gastner 1971), which measures CO₂ pressure during a hydrochloric acid attack. For the
160 calculation of the calcium carbonate percentage, see Appendix A in Peybernes et al. (2013).

161 Twenty-five dark shaly marlstone samples from the Takoucht section were selected for organic
162 matter analysis. Total organic carbon content (TOC), and the nature and thermal maturation of
163 organic matter were estimated using a Rock-Eval 6 Turbo apparatus (Vinci Technologies) at
164 UPMC–University of Paris 6. The method, described in detail by Behar et al. (2001), consists
165 of a two steps analysis with programmed temperature: a pyrolysis between 300 and 650°C
166 (25°/min), under an inert atmosphere (He), followed by oxidation between 300 and 850°C
167 (20°/min). All those parameters allow the calculation of the TOC, which is expressed as wt%
168 of bulk rock samples. The hydrogen index (HI), corresponds to the quantity of hydrocarbon
169 compounds released during the pyrolysis relative to the TOC (S2/TOC) in mg of HC per g of
170 TOC, and the Oxygen Index (OI, in mg CO₂/g TOC) is related to the amount of oxygen in the
171 kerogen and is normalized to the S3 value (S3/TOC). Although the source of organic matter is
172 usually defined by the mean of elemental analysis, the HI and OI parameters approximate
173 respectively the H/C and O/C atomic ratios, which are the determining factor for organic matter
174 characterization. The production index (PI) shows the level of thermal maturation. Tmax (°C)
175 is defined as the pyrolysis temperature at which the maximum amount of hydrocarbons is
176 yielded by kerogen. Tmax increases linearly with the natural maturation degree of the organic
177 matter, thus giving a rapid estimate of the thermal maturity of sedimentary basins (Espitalié et
178 al, 1985-1986; Dellisanti et al., 2010). The measurement accuracy is of ± 0.05% for TOC, ± 2°C
179 for Tmax, and ± 10 for HI and OI. Values are reported in the Appendix.

180 **III.3. Calcareous nannofossils**

181 Calcareous nannofossils were studied in 139 samples from Ida w Shayq, Tiskatine, Anzate and
182 Tinfoul sections. Samples were prepared using the random settling technique of Geisen et al.
183 (1999), adapted from Beaufort (1991), which allows the calculation of absolute abundances
184 (number of specimens per gram of rock). Nannofossils were observed at 1560 x magnification
185 using a polarizing light microscope,. At least 300 specimens per sample, both coccoliths and
186 nannoliths, were generally counted in a variable number of fields of view (a mean of 446, 369,
187 402, and 497 for the Anzate, Ida w Shayq, Tinfoul and Tiskatine sections, respectively). An
188 amount of 300 counted specimens is generally considered to be sufficient to have a good
189 estimation of species richness in one sample; in addition, the number of fields of view required

190 to count 300 specimens allows an estimation of the nannofossil abundance (Bown and Young,
191 1998). In 20 samples (9, 5, 3, and 3 samples from Anzate, Ida w Shayq, Tinfoul and Tiskatine,
192 respectively), less than 300 nannofossils (from 1 up to 208 specimens) were counted, due to the
193 paucity and poor preservation of nannofossils. All nannofossils with at least more than half of
194 the specimen preserved were counted. Both nannofossil total absolute abundance and relative
195 abundances of some key taxa were calculated for each sample. In these calculations,
196 *Nannoconus* spp. were excluded from the total sum of nannofossils because of their uncertain
197 biological affinity (Aubry et al., 2005). The taxonomic frameworks of Perch-Nielsen (1985)
198 and Burnett et al. (in Bown, 1998) were followed. The nannofossil preservation was evaluated
199 following the classes defined by Roth (1983).

200 Calcareous nannofossils are used in this study to better constrain the paleoenvironmental
201 conditions, in particular, trophic levels in the water column, pelagic carbonate production and
202 sea-surface temperatures. Calcareous nannofossil primary productivity is an indicator of trophic
203 levels in the water column; it is estimated here both with total absolute abundance and relative
204 abundances of fertility indicators such as *Biscutum* spp., *Discorhabdus rotatorius*,
205 *Lithraphidites carniolensis* and small *Zeugrhabdotus* spp. (Table 2; Peybernes et al., 2013).
206 The relative abundances of both *Nannoconus* spp., which constitute the biggest nannofossil
207 carbonate calcifiers and of calcareous nannofossil sea-surface temperature indicators were
208 calculated. Calcareous nannofossils considered as high latitude taxa (*Crucibiscutum* spp.,
209 *Repagulum parvidentatum*, *Rhagodiscus angustus* and *Seribiscutum* spp.; Table 2) were
210 considered in this study.

211

212 IV. RESULTS

213 IV.1. Ammonite biostratigraphy

214 In the EAB, Aptian and Albian ammonites have been first reported by Brives (1905), Lemoine
215 (1905), Gentil (1905), Kilian and Gentil (1906, 1907) and Roch (1930). While carrying out a
216 regional stratigraphic synthesis of the EAB, Ambroggi (1963) listed Cretaceous ammonite
217 specimens, collected unit by unit and identified by Breistroffer (e.g., Ambroggi and Breistroffer,
218 1959). Later, Wiedmann et al. (1978, 1982), Rey et al. (1986, 1988), Andreu (1989) and Witam
219 (1998) brought new precisions on ammonite occurrences. Since then, E. Robert (*in* Peybernes
220 et al., 2013) and L. Bulot (*in* Luber et al., 2017; 2019) refined the ammonite biostratigraphy of
221 the Aptian–lower Albian succession of the EAB.

222 In this work, since many new species and genus have been identified, and the lower part of the
223 successions is locally highly condensed, the presented biozones are accurate but preliminary,
224 pending on careful taxonomic revision (Giraud, Robert et al., in progress). In spite of the
225 absence in our collected samples of many of the zonal markers, we were able to correlate the
226 ammonite successions of the EAB with those of the Mediterranean and Tethyan regions, and
227 thus with the standard biostratigraphic ammonite zones (Reboulet et al., 2018). Although latest
228 Barremian ammonites are present (Jaillard et al., 2019), earliest Aptian specimens from the
229 *Deshayesites oglanlensis* Zone have not been found in the recently studied Aoulkjdad and
230 Takoucht sections, confirming a hiatus of this interval (Peybernes et al., 2013, Luber et al. 2017).

231 Early Aptian times are poorly represented, and were best studied in the northern sections. There,
232 the *Deshayesites forbesi* Zone has been tentatively identified by the presence of *Deshayesites*
233 *consobrinus*, associated with *Ancyloceras* sp. and first cheloniceratids (*Prochelonicer* sp. and
234 *Chelonicer* sp.). The *Deshayesites deshayesi* Zone is marked by the occurrence of
235 *Deshayesites deshayesi*, *D. consobrinoides*, *D. cf. grandis*, *Pseudohaploceras* sp., numerous
236 cheloniceratids specimens (among which *Prochelonicer* spp., *Chelonicer* *cornuelianum*, *C.*
237 *meyendorfi*) and the *Ancyloceras* genus, among which *A. cf. matheronianum*. The subsequent

238 *Dufrenoyia furcata* Zone is identified because of the presence of *Dufrenoyia furcata*,
239 *Australiceras* sp. and *Toxoceratoides emericianum*.

240 Late Aptian times are well represented in almost all sections. The *Epicheloniceras martini* Zone
241 is identified by the appearance of numerous specimens of the *Epicheloniceras* genus (*E. martini*,
242 *E. tschernyschewi*), together with *Colombiceras crassicostatum* and other species of the genera
243 *Vectisites*, *Neodufrenoyia* gen. nov. and *Colombiceras*. The upper part of the *E. martini* Zone
244 is marked by a well correlatable horizon bearing abundant *Australiceras* and
245 *Pseudoaustraliceras* (“Tropaeum beds” of the literature).

246 The *Parahoplites melchioris* Zone is poorly represented in the EAB. The association of
247 *Acanthohoplites* sp., *Colombiceras discoidales* and *Valdedorsella akuschaense* is tentatively
248 ascribed to this zone. In overlying strata, the *Acanthohoplites nolani* Zone and subsequent zones
249 present a fairly high faunal diversity.

250 The *Acanthohoplites nolani* Zone is represented in all sections and the historical, long
251 recognized “nolani bed” represents a good correlation level. Bulot and Latil (2014) called into
252 question the use of *A. nolani* as a zone index, and Luber et al. (2017) pointed out the
253 misidentification of this species for the Moroccan representatives, and introduced the species
254 *Esaisabellia tiskatinensis*. Nevertheless, we will follow the current standard zonation, awaiting
255 for next discussions of this purpose by the Kilian Group. In the “*A. nolani*” zone, the associated
256 fauna consists of *Epicheloniceras clansayense*, *Aconeceras aptiana*, *Pseudohaploceras* sp.,
257 *Diadochoceras* sp., *Zuercherella* sp. and specimens of the *Neodufrenoyia* gen. nov. and
258 *Acanthohoplites* genera (among which *A. bergeroni*, *A. Bigoureti anthulai*).

259 The *Hypacanthoplites jacobi* Zone is mainly represented by pyritous ammonites, and is defined
260 by the first occurrence of *Hypacanthoplites* spp. (*H. nolaniformis*, *H. elegans*, *H. clavatus*).
261 They are associated with *Epicheloniceras clansayense*, *Pseudorbulites convergens*,
262 *Phylloceras* (*Phylloceras*) *aptiense*, *Diadochoceras migneni*, *Parasilesites kilianiformis*, and
263 representatives of the genera *Eogaudryoceras*, *Falotermiericeras* gen. nov., *Neodufrenoyia*,
264 first *Phyllopachyceras* and *Eogaudryoceras* (*Eotetragonites*).

265 Earliest Albian times are well represented, although the corresponding fauna is poorly
266 preserved. The *Leymeriella tardefurcata* Zone is characterized by the occurrence of various
267 specimens of Silesitoidinae and of the genera *Phylloceras*, *Phyllopachyceras*,
268 *Hypacanthoplites*, *Mellegueiceras*, *Paragonoceras*, *Uhligella*, *Puzosia*, *Eogaudryoceras*
269 (*Eotetragonites*) together with *Douvilleiceras leightonense*, *Oxytropidoceras*
270 (*Oxytropidoceras*) sp., *O. (Mirapelia) mirapelianum*, *Neosilesites palmensis*, *Ptychoceras*
271 *laeve*, *Parabrancoeras* sp. and other less representative or endemic specimens. Mainly
272 because of poor outcrops in a chiefly argillaceous series, the *Douvilleiceras mammillatum*
273 Superzone is less represented. However, the occurrence, among others, of *Douvilleiceras*
274 *mammillatum aequinodum*, *Prolyelliceras gevreyi*, *Beudanticeras dupinianum africana*, *B.*
275 *revoili*, *Uhligella rebouli*, *Paragonoceras bussoni* and *P. hachourii* characterizes this time
276 span. The “Beudanticeras beds” (Roch, 1930; Ambroggi, 1963) mostly belong to this interval.

277 Toward the West (Tamri, Imsouane), the Aptian–lower Albian series is condensed in a
278 phosphate- and glauconite-rich, conglomeratic level, which contains ammonites of early Aptian
279 to earliest Albian age (Robert, in Peybernès et al., 2013).

280 **IV.2. Sedimentary facies**

281 Aptian facies differ from those of the uppermost Aptian–lower Albian series, in their lithology
282 and detrital quartz content, as well as in their faunal content.

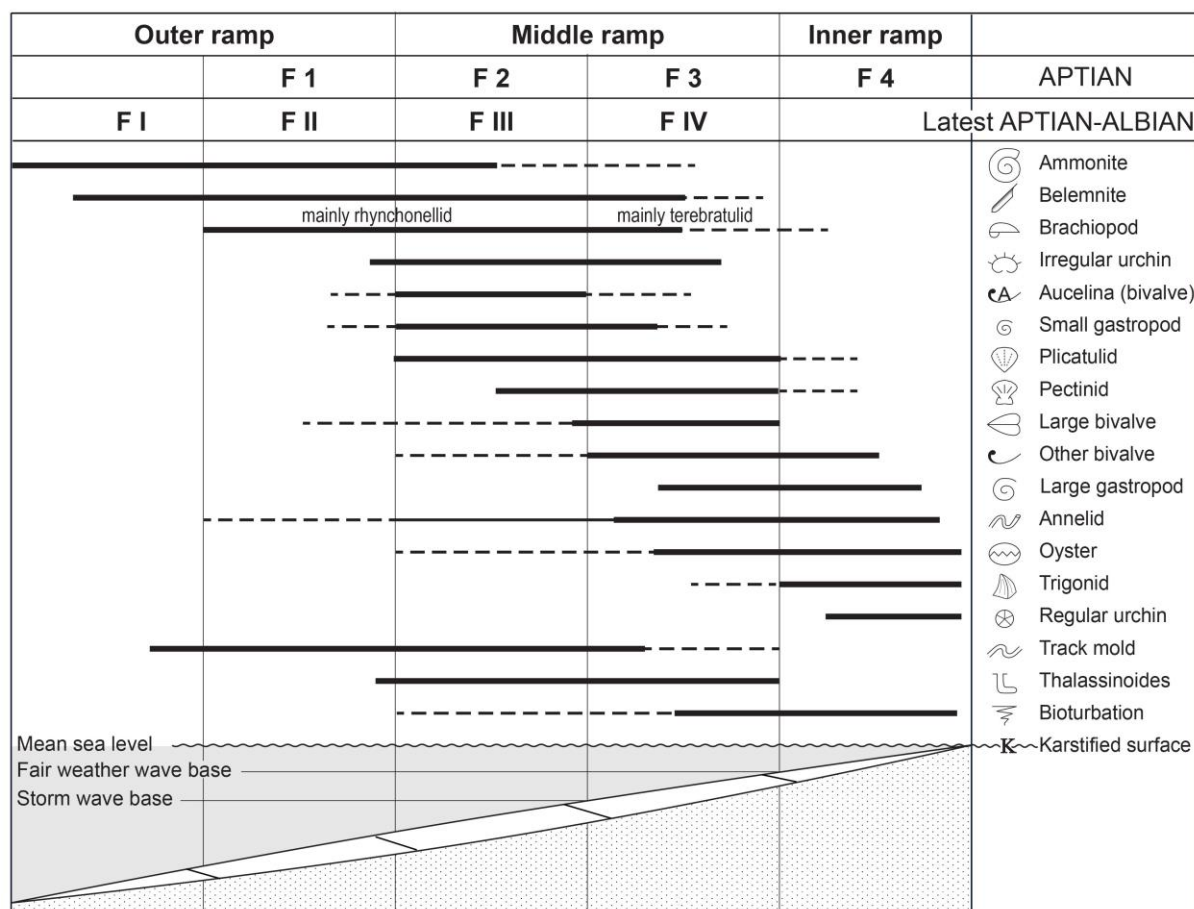
283 **IV.2.1. Aptian facies** (Fig. 3)

284 **Facies 1 (F 1):** Facies 1 is made of shales or shaly marlstone, containing mainly belemnites and
 285 some ammonites. Sandstone or marl beds are almost absent (less than 5% in thickness). Scarce
 286 thin-shelled bivalves, annelids (serpulids) and small-sized gastropods may occur. Because of
 287 the shaly nature of the deposits, bioturbation is hardly visible. Ammonites may be pyritous.

288 *Interpretation:* The lack or scarcity of carbonate suggests that sedimentation took place far from
 289 the “carbonate factory” (Tucker and Wright, 1990; Schlager, 2003) located in the nearshore
 290 euphotic zone, where photosynthesis favours the organic activity of carbonate generating
 291 organisms (from bacterias to algae and molluscs). The strong predominance of pelagic
 292 organisms and the scarcity of benthic fauna suggests a deposition below the euphotic zone.
 293 Therefore, facies F1 is interpreted as characterizing distal outer shelf deposits.

294 **Facies 2 (F 2):** Facies 2 consists of shales or shaly marlstone, with some marly beds (about 20-
 295 30 % of total thickness). The faunal content is dominated by belemnites, ammonites, irregular
 296 sea urchins, brachiopods (terebratulids) and plicatulids, associated with some gastropods,
 297 bivalves (mostly thin-shelled), annelids and scarce nautiloids. Isolated corals locally occur.
 298 Bioturbation consists of track molds, small sized curved burrows and digging traces (sediment
 299 feeders), mainly visible in the marlstone beds.

300 *Interpretation:* The occurrence of benthic, relatively deep water organisms (e.g. echinoids,
 301 brachiopods), together with planktonic fauna (cephalopods) suggests a hemipelagic
 302 environment. The lithological association (prevailing marl, subordinate limestone) also points
 303 to an outer shelf setting. Bioturbations are dominated by the activity of sediment feeders,
 304 suggesting an outer shelf environment and moderately oxygenated conditions.



305
 306 *Figure 3. Sedimentary facies of the Aptian (A) and uppermost Aptian–Lower Albian (B) along the*
 307 *ramp of the Essaouira-Agadir basin.*

309 **Facies 3 (F 3):** Facies 3 is made of marly limestones (about 30-50% of total thickness) with
 310 marly interbeds. The faunal content is dominated by benthic organisms, such as brachiopods,
 311 annelids and bivalves, among which oysters, plicatulids, pectinids and thick-shelled large
 312 bivalves. Ammonites occur commonly. Bioturbation dominantly consists of burrows (curved
 313 and straight) and track molds.

314 *Interpretation:* The predominance of a diversified benthic fauna indicates a shallow, open
 315 marine environment, while the abundance of limestone suggest the proximity of the “carbonate
 316 factory” and hence, of a carbonate platform. However, the lack of algae and of very shallow
 317 organisms or features (e.g. oncolites, rudistids, corals) precludes a very shallow environment.
 318 The dominance of burrows and surficial track molds supports the interpretation of a shallow
 319 (proximal) open shelf environment.

320 **Facies 4 (F 4):** This facies is lithologically marked by thick, massive limestone beds, containing
 321 shallow marine benthic bivalves, such as abundant oysters, some trigonids and scarce rudistids.
 322 Bioclasts are common and belemnites may occur at the top of these beds. Bioturbation is
 323 represented by burrows. The top of these beds is locally karstified (see surface S1, below).

324 *Interpretation:* The predominance of a shallow marine benthic fauna indicates a shallow
 325 carbonate shelf environment. Evidence of frequent emergence at the top of these deposits
 326 support this interpretation. The presence of bioclasts suggests a moderate energy environment,
 327 which is supported by the predominance of suspension feeders. F4 sediments are thus
 328 interpreted as deposited in a well oxygenated, shallow to very shallow carbonate shelf
 329 environment, with moderate energy.

330 **IV.2.2. Uppermost Aptian–Albian Facies (Fig. 3)**

331 **Facies I (F I):** Facies I is made up of monotonous, dark-coloured, almost azoic shales or shaly
 332 marlstones. Long searches on these outcrops allowed only to find scarce ammonite casts.

333 *Interpretation:* The lack of fauna and sedimentary structures makes any reliable interpretation
 334 difficult. However, as this facies usually overlies or underlies the FII facies, is devoid of benthic
 335 fauna, and occurs at the top of the studied sections, it is interpreted as a pelagic, deep water
 336 marine deposit.

337 **Facies II (F II):** Facies II is very comparable to the F 1 facies, and consists of silty shales or
 338 silty shaly marlstone, containing mainly belemnites and some ammonites. Sandstone beds are
 339 virtually absent (less than 5 % of the total thickness). Scarce thin-shelled bivalves, annelids,
 340 plicatulids, small sized gastropods and brachiopods (mostly rynchonellids) occur sporadically.
 341 Because of the shaly nature of the deposits, bioturbation seems to be absent, except in the
 342 sandstone or marlstone beds, where digging tracks dominate.

343 *Interpretation:* The lack, or scarcity, of carbonate suggests that sedimentation took place far
 344 from the carbonate factory, i.e. in a distal place, if the carbonate content is due to export from
 345 shallow water deposits. The strong predominance of pelagic organisms and the scarcity of
 346 benthic fauna support a deposition depth below or near the lower limit of the euphotic zone.
 347 Therefore, facies F II is interpreted as a hemipelagic deposit, in a distal outer shelf environment,
 348 and is thought to be roughly equivalent to the F 1 facies.

349 **Facies III (F III):** Facies III is made of shales or shaly marls, with thin beds of sandstone or
 350 sandy marl (about 30 % of the total thickness). The faunal content is dominated by belemnites,
 351 ammonites and brachiopods (mostly terebratulids), associated with some gastropods,
 352 plicatulids, and thin-shelled bivalves. Bioturbation in the sandstone beds consists of small sized
 353 curved burrows and digging traces (sediment feeders).

354 *Interpretation:* The occurrence of benthic, relatively deep water organisms (e.g. brachiopods,
355 plicatulids), together with planktonic fauna (cephalopods) suggests a hemipelagic environment.
356 The lithological association (prevailing silty to sandy marlstone) also points to an outer shelf
357 setting, comparable to that of Facies F 2. However, the presence of sediment feeders, even in
358 the sandstone beds, suggests that sea bottom waters were less oxygenated than in Facies 2.

359 **Facies IV (F IV):** F IV consists of yellow, dolomitic, well-sorted sandstone beds, usually
360 separated by silty to marly interbeds. The faunal content is dominated by benthic organisms,
361 such as brachiopods (terebratulids) and bivalves, among which gastropods, oysters, plicatulids,
362 pectinids and other bivalve fragments. Ammonites and belemnite fragments are common.
363 Sedimentary structures such as current ripples and cross-bedding are also common. The lower
364 part of the dolomitic sandstone beds is commonly rich in varied reworked elements: phosphatic
365 fragments, internal molds of gastropods or ammonites, brachiopods, lithoclasts and belemnite
366 rostra. Bioturbation consists of burrows (curved and straight), track molds and digging traces.
367 F IV commonly overlies erosional surfaces, below described as S 4.

368 *Interpretation:* The predominance of a diversified benthic fauna indicates an open marine
369 environment. The occurrence of current-related structures indicates a moderate to high energy
370 during deposition, which is supported by the good sorting of sandstone grains. The abundance
371 and diversity of bioturbation, as well as the energetic conditions, support the interpretation of a
372 shallow (proximal) outer shelf environment, probably above the fairweather wave base. When
373 F IV deposits overly S 4 surfaces, they are interpreted as resulting from the decreasing intensity
374 of submarine currents responsible for the erosional surface. As these currents decrease, they
375 allow deposition of sandstones, mixed with reworked elements, both brought out from the
376 underlying, eroded strata. When F IV does not overly S 4 surfaces, it may be interpreted as
377 storm deposits, resulting from an abrupt detrital supply derived from littoral areas, possibly
378 related to river floods, or resulting from high frequency relative sea-level drops.

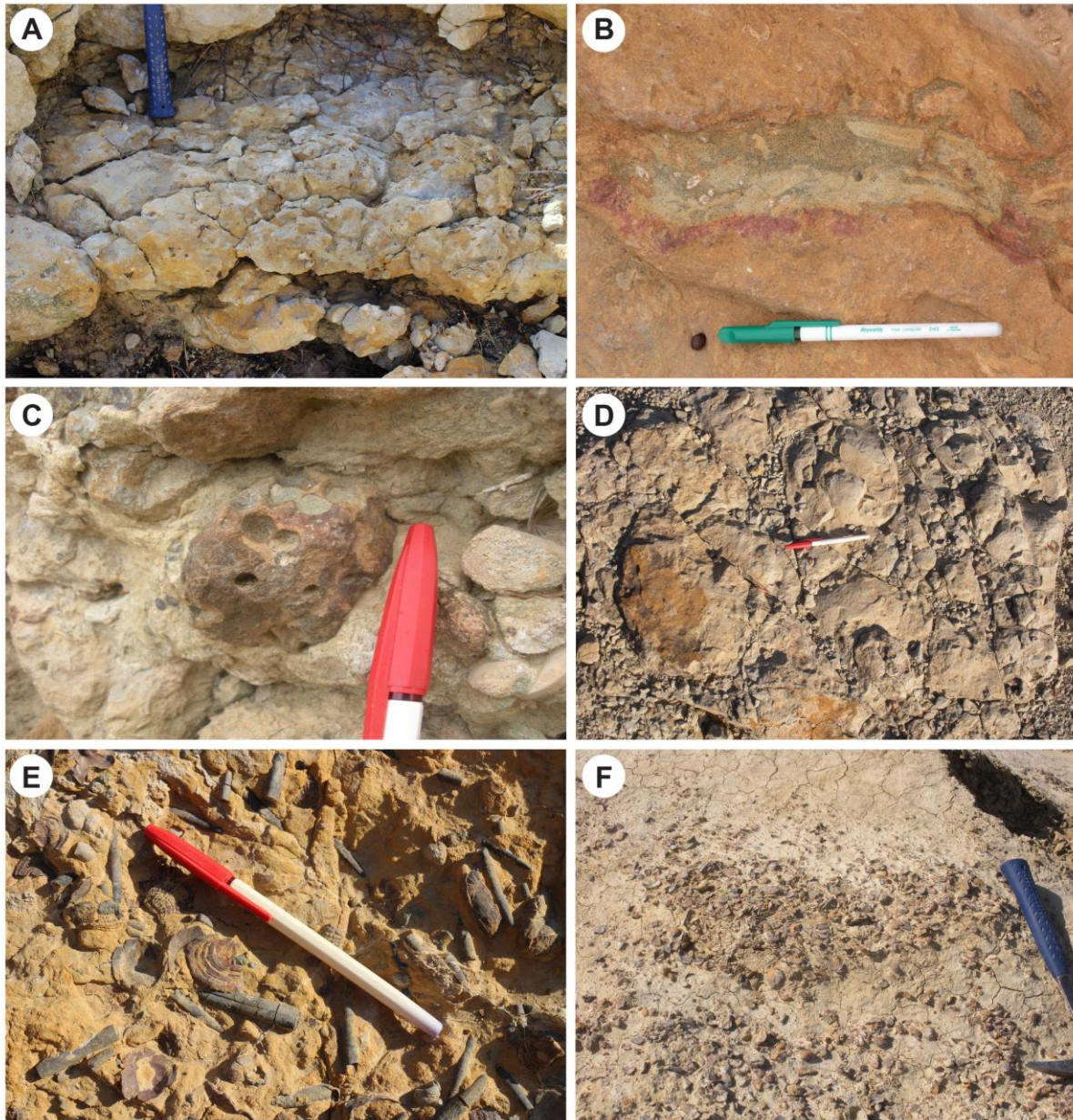
379 **Facies D (F D):** Facies F D is characterized by a poor faunal diversity, together with the high
380 abundance of one type of organism, usually annelids (serpulids) or buchidae bivalves (e.g.
381 *Aucellina* sp.). F D is usually associated with monotonous shales or shaly marlstones, or with
382 alternating marlstone /silty marlstone and marlstone /sandstone, with predominance of
383 marlstones or silty marlstones (lithologies of F 1, F 2, F II or F III). Bioturbation is sparse, but
384 this may be due to the shaly lithology. Pyrite is commonly abundant.

385 *Interpretation:* The poor faunal diversity, the presence of pyrite and the predominance of
386 organisms tolerating oxygen-depleted environments (buchidae, serpulids, De la Mora et al.,
387 2000; Henderson, 2004) point to dysaerobic conditions. However, the occurrence of scarce
388 bioturbation indicates that benthic life was still possible, and therefore, that conditions were not
389 anoxic. Because of the scarcity of other fauna, the depositional environment is difficult to assess
390 precisely, and it will be interpreted based on the lithology. For this reason, the dysaerobic facies
391 (F D) will be named based on their lithology, for instance F 2D or F IID. In all cases, in the
392 studied sections, F D is of restricted to outer shelf environments.

393

394 **IV.3. Peculiar sedimentary surfaces**

395 **Surface 1 (S 1):** The first type of surface is usually found on top of a massive limestone bed. It
396 is an uneven, corroded surface, the cavities of which are filled by the overlying highly
397 glauconitic deposits, or by iron oxydes (see below) (Fig. 4A, 4B). The centimeter-scale cavities
398 may penetrate in the limestone beds as much as several tens of centimeters deep. In the upper
399 surface of the bed, the calcite of bioclasts has been locally dissolved and is replaced by iron
400 oxydes, iron-rich dolomite or by glauconitic-rich sediments.



401

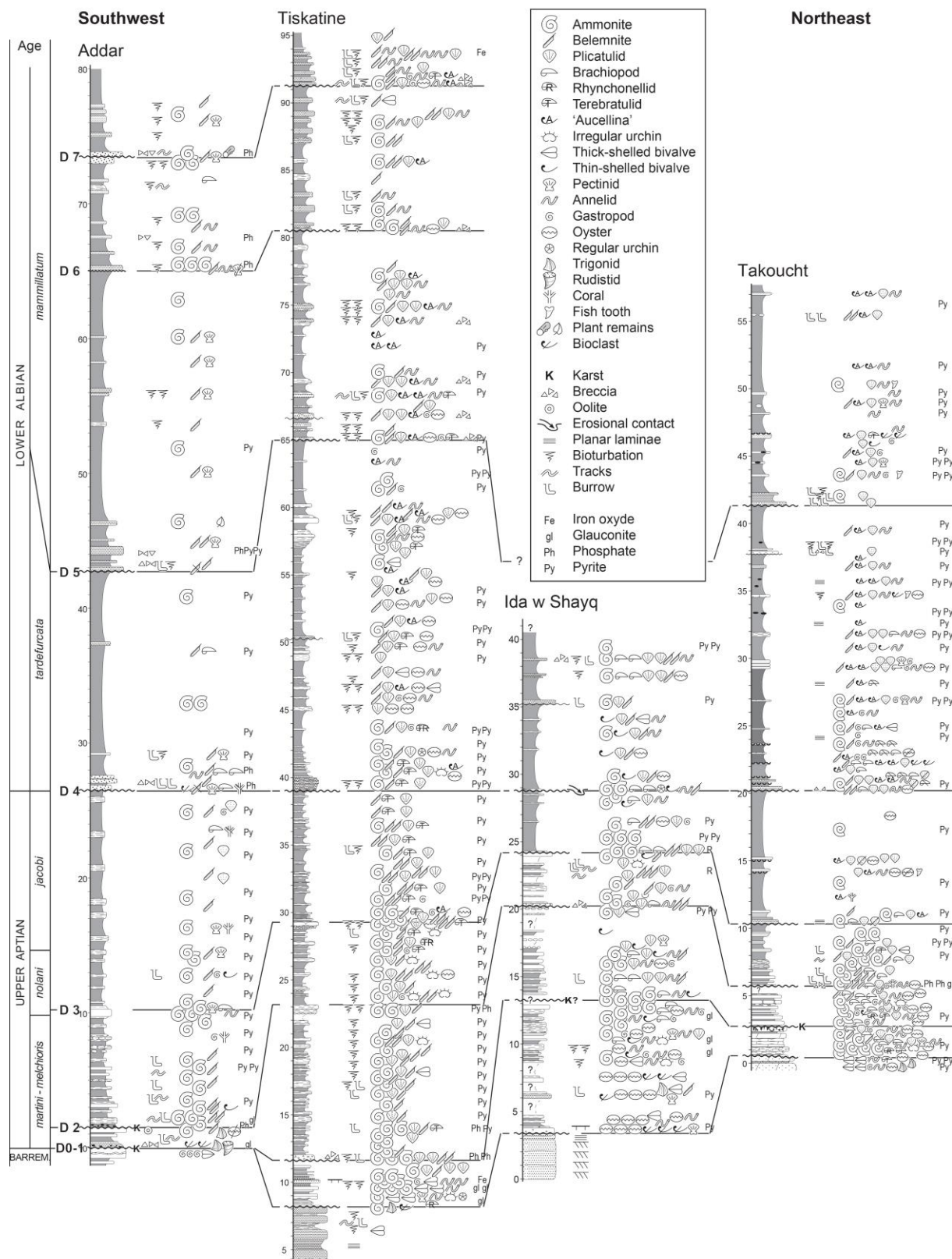
402 *Figure 4. Types of sedimentary surfaces in the Essaouira-Agadir basin. A. Karsted surface S1 (D1,*
 403 *Takoucht section). B. Glauconitic infilling of a karstic cavity on a S1 surface (D1, Addar section). C.*
 404 *Bored rounded clast in a phosphatic conglomerate (S2 surface, Tamri section). D. Iron oxide rich*
 405 *crust (S3 surface, D3, Addar section). E. Concentration of belemnites and plicatulids and gastropod*
 406 *shells at the base of a dolomitic sandstone bed (S4B surface) (D4, Taounerine section). F. S4A surface*
 407 *marked by a concentration of brachiopods and plicatulids shells in a marly succession (D4, Ida w*
 408 *Shayq section).*

409

410 *Interpretation:* S1 is interpreted as a karstified surface, which indicates a period of subaerial
 411 exposure and explains the dissolution by meteoric water. S1 is, therefore, interpreted as a
 412 sequence boundary (SB). It is only found at the base of the studied sections (i.e. in lower Aptian
 413 deposits), and mainly in the southern part of the basin, where several S 1 surfaces may be
 414 amalgamated. In the latter case, reworked ammonites of different ages suggest large time gaps.

415 **Surface 2 (S 2):** The second type of surface is represented by a thin layer of highly glauconitic,
 416 sometimes phosphatic deposits that commonly form a crust. It commonly contains lithoclasts,
 417 fossils and bioclasts (oysters, brachiopods, gastropods, belemnites, ammonites) of various

418 nature and origin. It may fill the karstic cavities and depressions of S1, or form a distinct layer.
 419 In some cases, large lithoclasts are bored (Fig. 4C).



420
 421 *Figure 5. North-South correlations of some Aptian-lower Albian sections of the Essaouira-Agadir*
 422 *basin.*

423 *Interpretation:* S 2 is thought to represent a condensed deposit, resulting from a submarine
424 hiatus. The occurrence of a variety of organisms living in shallow to moderately deep
425 environments suggests that condensation partly occurred in a shallow marine environment. This
426 is supported by the local presence of bored clasts, boring being restricted to shallow marine
427 environments and being common in tidal environments. However, the presence of glauconite
428 and phosphate suggests that at least part of the condensation occurred in an outer shelf
429 environment, likely related to mineralised, deep water currents. S 2 is, therefore, interpreted as
430 related to a transgressive episode. S 2 is usually found at the base or at the top of the studied
431 sections, and only in the western part of the basin.

432 **Surface 3 (S 3):** Surface 3 is marked by a thin, discontinuous, iron-rich crust, which covers the
433 upper surface of marly or calcareous beds (Fig. 4D). It is locally associated with some small-
434 sized lithoclasts, and concentrations of pelagic fauna (cephalopods). It is mainly recorded in the
435 upper Aptian deposits.

436 *Interpretation:* S 3 is interpreted as a hard ground representing a submarine hiatus, likely related
437 to marine currents. In upper Aptian deposits, S 3 commonly laterally evolves to S 4 surface
438 (submarine erosion, see below). In this case, S 3 is interpreted as resulting from the
439 mineralization by submarine currents of a hard bed (calcareous marlstone or limestone) that
440 resisted to the submarine erosion, the latter having removed the underlying shales and being
441 still active elsewhere. In the western, condensed sections, S 3 may be merged with S 1 or S 2
442 surfaces.

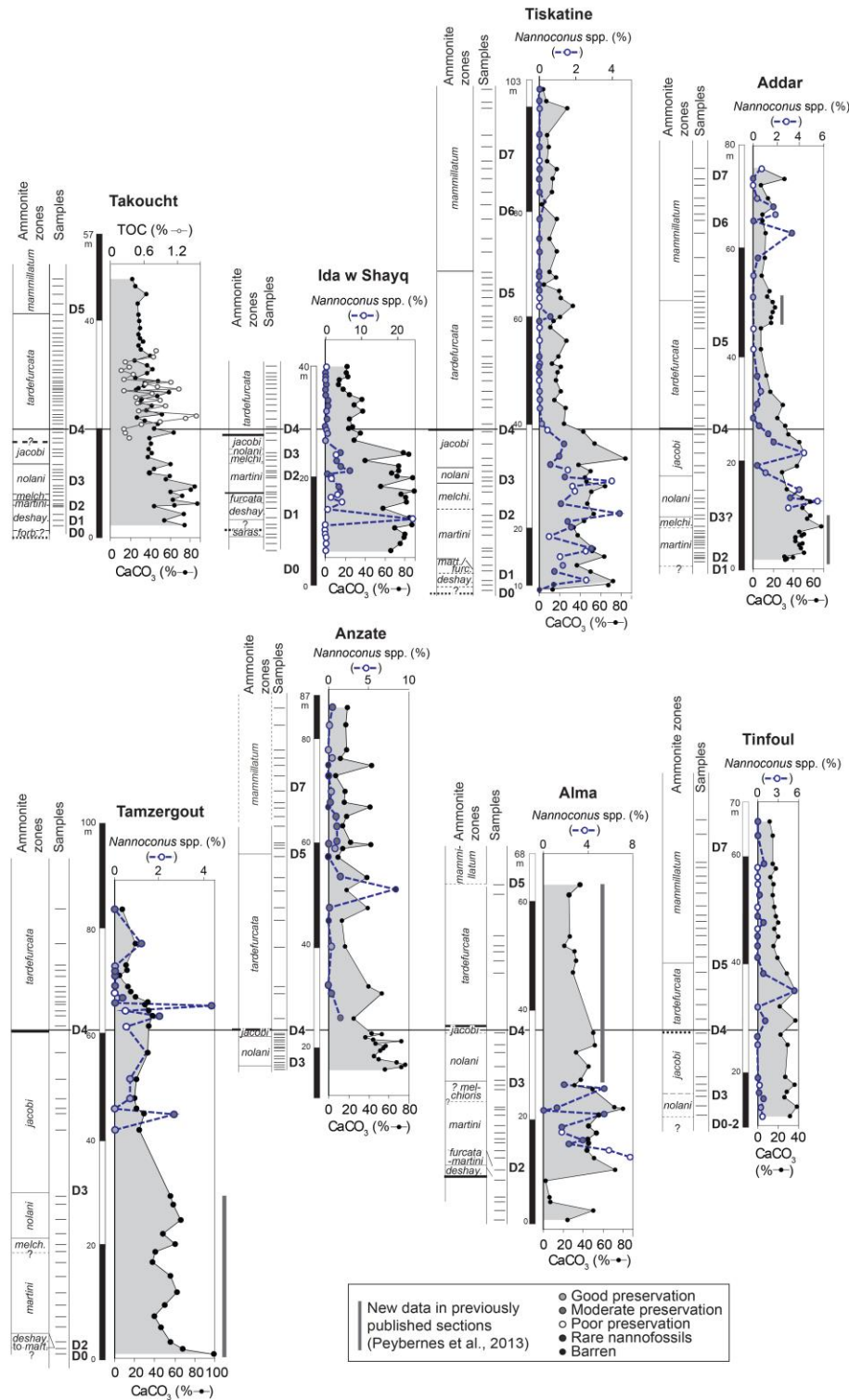
443 **Surface 4 (S 4):** An other type of surface is found at the base of high concentrations of
444 belemnites rostra associated with lithoclasts, flat pebbles, phosphatized white internal molds of
445 fossils (commonly gastropods and ammonites) and scarce other bioclasts (Fig. 4E and 4F).
446 These elements can be found, either as coquina layers within a marly shale succession (S 4A),
447 or reworked at the base of, or within, limestone or calcareous sandstone beds (S 4B) (see Fig.
448 5). In the first case (S 4A; Fig. 4F, and D4 in Ida w Shayq section on Fig. 5), these coquinas are
449 frequently lenticular in shape, since they overlie a slightly uneven surface, and may be
450 associated with fine-grained sand. Where the coquina is lacking, S 4 may be only marked by a
451 slight lithological change, associated with an upward change in the faunal content, from pelagic
452 organisms to assemblages including benthic species. In the second case (S 4B; Fig. 4E), clasts,
453 bioclasts and molds are concentrated at the base of the overlying bed, and rapidly disappear
454 upward. S 4 occurs in the uppermost Aptian and lower Albian succession.

455 *Interpretation:* S 4 may be interpreted in two distinct ways. In the most common case, the
456 reworked faunal assemblage, as well as the overlying one, contain pelagic organisms. Such an
457 erosional surface is interpreted as representing a submarine hiatus, associated with erosion of
458 the underlying marlstone or shale, related to relatively strong submarine currents. In this
459 interpretation, the submarine erosion would have removed the small-sized sedimentary
460 particles (shale, marlstone), thus bringing out and concentrating their detrital and pelagic faunal
461 content. The frequent occurrence of phosphatic internal molds of organisms suggests that
462 upwelling currents played a role in this erosion and allowed phosphatisation of carbonate
463 elements during the erosional hiatus. However, since the S 4 surface is always found at the top
464 of shaly or marly series, the occurrence of emersion periods cannot be ruled out for some of
465 these surfaces. As a matter of fact, on one hand, the overlying bed may contain shallow water
466 fauna (oysters, trigonids, corals), and on the other hand, shale or marlstone cannot be karstified,
467 and possible evidences of subaerial erosion (e.g. paleosoils, fluvial or eolian sands, etc.) may
468 have been eroded, and removed or reworked by the overlying, transgressive high-energy
469 deposits.

470

471 **IV.4. Calcimetry and rock-eval pyrolysis**

472 For all successions, calcium carbonate values are higher in the Aptian than in the Albian deposits, with values generally comprised between 40% and 90% up to the end of the *A. nolani*
 473 ammonite Zone. Close to the Aptian–Albian boundary, the calcium carbonate content sharply
 474 decreases, and remains low or slightly decreases through early Albian times (Fig. 6).
 475



476

477 *Figure 6. Stratigraphic changes in calcium carbonate content and relative abundances of Nannoconus*
 478 *spp. for the different sections. For the Takoucht section, the TOC is added. The sedimentary*
 479 *discontinuities (D0 to D7) are indicated.*

480 In the Takoucht section, the 25 analyzed samples contain between 0.2 and 1.5% TOC, with an
481 average of 0.7%. There is no clear relationship between TOC% and CaCO₃% (Fig. 6), which
482 suggests that the percentage of organic matter does not result from its dilution by carbonate
483 input. Hydrogen indices are comprised between 128 and 198 mg/g of rock, Oxygen indices
484 from 159 to 311 mg/g, S1 from 0.01-0.05 mg/g, and S2 from 0.12 to 3.01 mg/g. The PI is
485 always very low with values in the range of 0.01 to 0.16. Temperatures of maximum pyrolytic
486 yield (Tmax) are in average of 438°C (Appendix), indicating that the organic matter did not
487 experience high temperature during burial. Thus, organic matter in the Takoucht section was
488 still immature with respect to petroleum generation. The very low free hydrocarbon content (S1
489 = 0.01-0.05 mg/g rock) confirms this immaturity. Such low maturation allowed the use of the
490 hydrogen index (HI) as an indicator of the origin and composition of the organic matter
491 (Espitalié et al., 1985-1986). According to the low range of the HI values, the organic matter
492 of the Takoucht section could be attributed to Type III, related to terrestrial higher plants debris
493 or to altered Type II, derived mainly from algae and/or bacteria, but highly oxidized.

494

495 **IV.5. Calcareous nannofossils**

496 Calcareous nannofossil total absolute abundance, relative abundances of calcareous nannofossil
497 fertility (meso-eutrophic taxa), sea-surface temperature indicators (cold taxa) and *Nannoconus*
498 spp. are plotted with the ammonite biostratigraphic information for each section. Calcareous
499 nannofossil data obtained from the present study (Ida w Shayq, Tiskatine, Anzate and Tinfoul)
500 are compared to those published from Addar, Tamzergout and Alma (Peybernès et al., 2013)
501 (Figs. 6 and 7). The lower part of the Alma succession contains many barren samples due to
502 dolomitization. This section is not shown in Figure 7, because the few scattered data do not
503 allow to comment any trend.

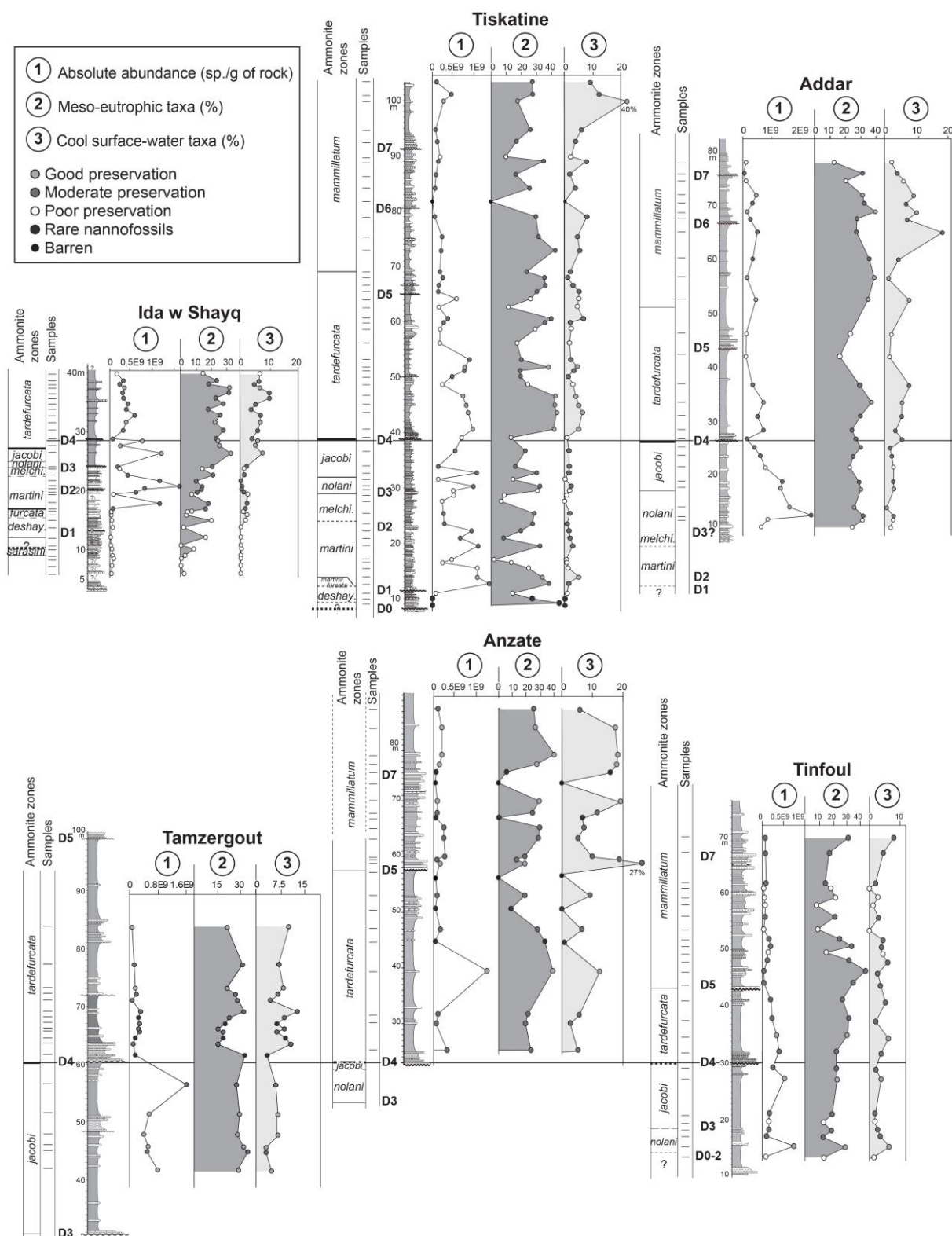
504 In the studied sections, preservation of calcareous nannofossils is poor to good and fluctuates
505 all along the successions (Fig. 7); some samples of both Tiskatine and Anzate sections are
506 barren of nannofossils and/or contain very rare nannofossils (Fig. 7). The means of the
507 nannofossil total absolute abundance are higher in the distal sections of Addar (0.57×10^9
508 specimens per gram of rock) Ida w Shayq (0.43×10^9), Tiskatine (0.35×10^9) and Tamzergout
509 (0.33×10^9), with respect to the more proximal sections of Anzate (0.18×10^9) and Tinfoul
510 (0.13×10^9). A progressive decrease in the nannofossil total absolute abundance is recorded
511 through the Aptian–early Albian interval, except for the Ida w Shayq section, which shows a
512 sharp decrease around the Aptian–Albian boundary (Fig. 7). The mean relative abundance of
513 meso-eutrophic taxa is comprised between 17.8 (Ida w Shayq) and 28.6% (Addar), which
514 represent relatively high values. The relative abundance of meso-eutrophic taxa follows an
515 opposite trend with respect to the nannofossil total absolute abundance, since it generally
516 increases in the latest Aptian and earliest Albian (between D3 and D5); in both Tamzergout and
517 Anzate the absence of data below this interval does not allow to observe this trend (Fig. 7).
518 Above D5 (*D. mammillatum* Superzone), the relative abundance of meso-eutrophic taxa
519 decreases (Fig. 7). In all sections except Tinfoul, an increase in the relative abundance of cold
520 taxa is recorded from the late Aptian to the early Albian, and the Anzate section shows higher
521 percentages than the other ones (Fig. 7). The relative abundance of the largest nannofossil
522 calcifier, *Nannoconus* spp., decreases from the late Aptian to the early Albian (Fig. 7). The
523 proximal Tinfoul section presents both the lowest *Nannoconus* spp. percentages and calcium
524 carbonate contents (Fig. 6).

525

526 **V. INTERPRETATIONS**

527 **V.1. Aptian–lower Albian depositional sequences**

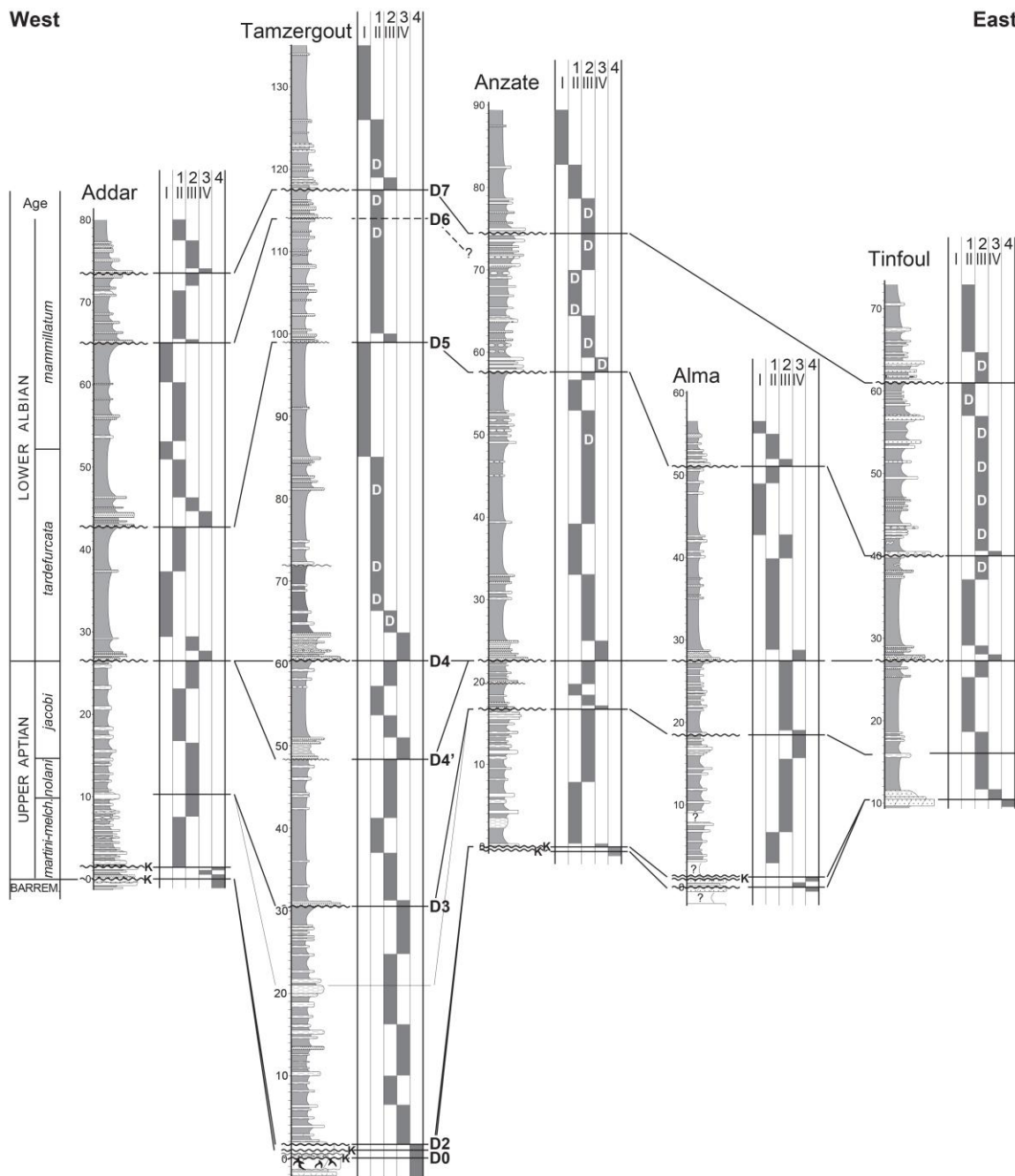
528 The identification of facies and discontinuity surfaces allowed us to define seven depositional
 529 sequences in the Aptian–early Albian interval (≈ 15 Ma).



530
 531 *Figure 7. Stratigraphic changes in calcareous nannofossil total absolute abundance and relative*
 532 *abundances of both meso-eutrophic and cold taxa. The sedimentary discontinuities (D0 to D7) are*
 533 *indicated.*

534 The **first sequence** (< 10 m) is only developed in the northern part of the EAB. In Ida w Shayq
 535 and Smimou, its lower part yielded latest Barremian ammonites (*M. sarasini* ammonite Zone,

536 Jaillard et al., 2019), whereas the upper part contains ammonites from the *D. deshayesi* Zone at
 537 Smimou, Ida w Shayq and Aoulkjedad. Its lower limit (D 0, Figs. 5, and 8 to 10) is an S 1-type,
 538 karstified surface.



539
 540 *Figure 8. East-West correlations of the Aptian-lower Albian sections in the southern part of the*
 541 *Essaouira-Agadir basin. D: dysaerobic facies. See Fig. 10 for caption, and Fig. 3 for explanation of 1*
 542 *to 4, and I to IV.*

543 At Ida w Shayq, parts of the section are covered, and it is possible that this sequence includes
 544 an additional, unobserved discontinuity. The lower, transgressive part of the sequence is
 545 dominated by marlstone and sandstone beds rich in oysters, with subordinate pectinids and
 546 trigonids. The middle part contains irregular urchins, associated with ammonites, oysters and
 547 serpulids, while the marly to calcareous upper part yielded mainly ammonites and brachiopods.
 548 Its top is usually represented by a remarkable accumulation of cheloniceratids (« *Cheloniceratid*
 549 *bed* »), locally exhibiting karstic dissolution (Ida w Shayq). These features indicate an overall

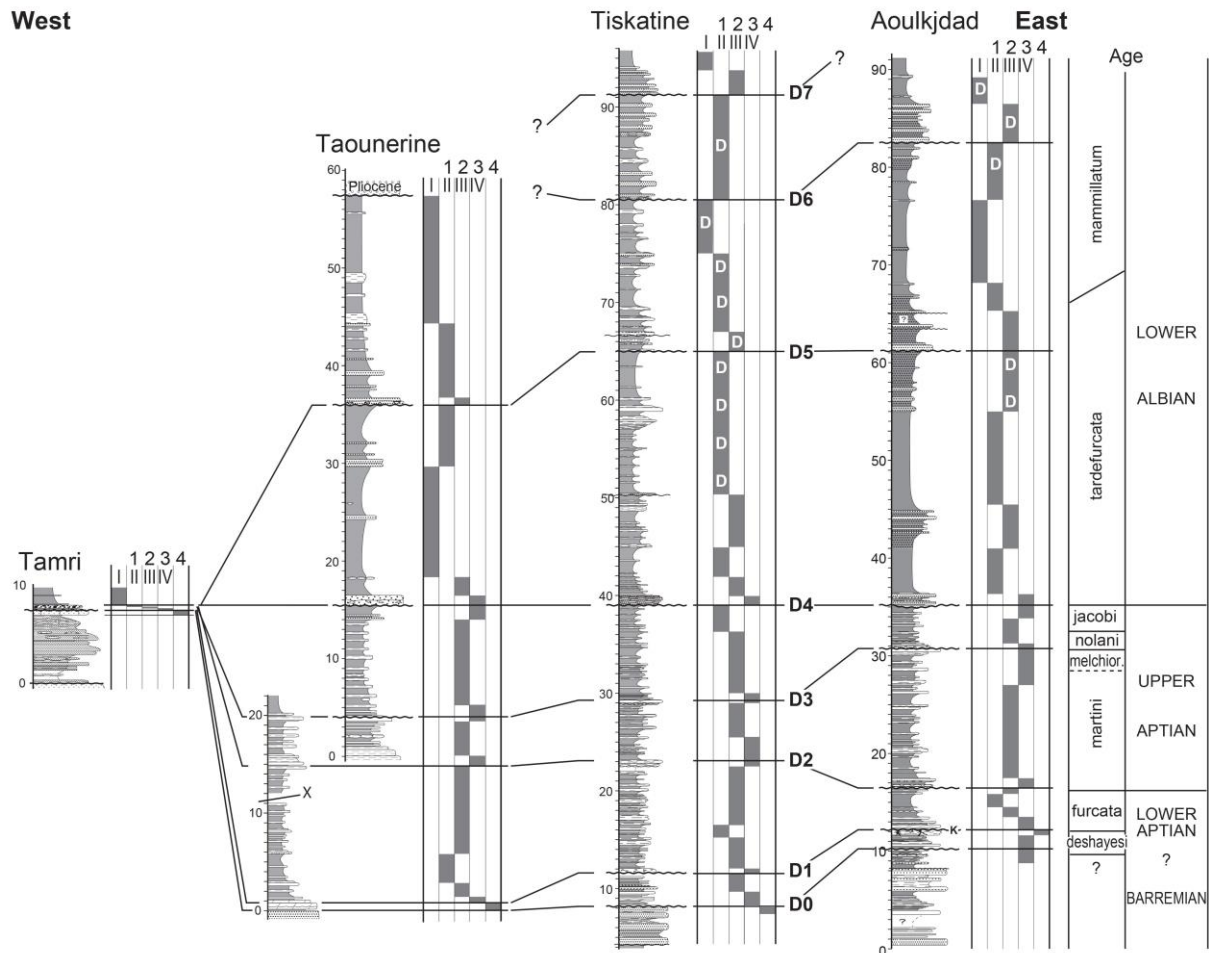
550 transgressive trend for the sequence. In the southern sections, this sequence may be represented
551 by the undated infilling of karstic cavities related to amalgamated emersion surfaces. This
552 sequence seems to roughly coincide with the Tamzergout Fm of Rey et al. (1988) and Witam
553 (1998).

554 The **second sequence** (< 11 m) is mainly observed in the northern part of the basin. In the Ida
555 w Shayq section, it yielded late early to early late Aptian ammonites (*D. deshayesi* ? to *E.*
556 *martini* zones). Its lower boundary (D 1, Figs. 5, and 8 to 10) is an S 1 surface in Takoucht, Ida
557 w Shayq and Aoulkjedad. There, it is marked by a thinning upward succession of limestone beds.
558 Whereas the lower part is dominated by ammonites and brachiopods, the shaly upper part
559 mainly contains plicatulids and scarce ammonites. This evolution is interpreted as a mainly
560 transgressive succession, the regressive part of the second sequence being eroded below the
561 upper discontinuity surface. In the Tiskatine and Aoulkjedad sections, it is represented by a
562 monotonous marlstone-limestone alternation, rich in plicatulids, belemnites and ammonites.
563 This sequence commonly ends with a limestone bed rich in large ammonites (« 'Tropaeum'
564 bed »). In the southern sections, the second sequence is usually represented by a massive
565 limestone bed intercalated between two emersion surfaces (S 1), whereas it is lacking in the
566 easternmost section (Tinfoul, Fig. 8).

567 The **third sequence** (< 14 m) is recorded in all sections. It yielded early late Aptian ammonites
568 (*E. martini*, to base of *A. nolani* zones). Its base (D 2, Figs. 5, and 8 to 10) is locally a S 4B
569 surface, consisting of a limestone bed rich in phosphatized fossils (Addar, Ida w Shayq).
570 Elsewhere, the base of the sequence is placed at the top of the "Tropaeum bed" (S 3 surface).
571 This sequence comprises a first thinning-upward, then thickening upward alternation of shaly
572 and calcareous marl beds. The fauna is dominated by belemnites, ammonites and plicatulids,
573 which are associated with oysters at the base, irregular urchins in the middle part, and
574 brachiopods at the top of the sequence. This faunal evolution supports a deepening-, then
575 shallowing-upward trend. In all sections, its top is clearly marked by a noticeable marly
576 limestone bed extremely rich in «*Nolaniceras*» spp. («*Nolani* bed »). The second and third
577 sequences appear to correspond to the Tadhart Fm (Rey et al., 1988; Witam, 1998).

578 The **fourth sequence** (< 5 to 30 m) crops out in all sections. It is well dated by latest Aptian
579 ammonites (*A. nolani* to *H. jacobi* zones). Its base (D 3, Figs. 5, and 8 to 10) is locally marked
580 by a slightly erosional sandy bed (Anzate Alma, Tamzergout, Takoucht). At Aoulkjedad, it
581 consists at the base (S 4B) of a bed rich in phosphatized ammonites and bioclasts. Elsewhere,
582 it is marked by the oxydized top of the «*Nolani* bed » (S 3). In Takoucht, a low angular
583 unconformity can be seen between the sandstone bed (S 4 surface) and the «*Nolani* bed » (S 3
584 surface), thus evidencing submarine erosion, which took place during the hiatus causing the
585 sequence boundary (Fig. 10). The fourth sequence is usually a thinning-upward, mainly marly
586 succession, rich in ammonites, belemnites and plicatulids. According to the sections, thin
587 sandstone beds are present (Addar, Anzate, Taounerine), some ammonites are pyritous (Anzate,
588 Taounerine), and calcareous beds appear in the upper part of the sequence (Ida w Shayq),
589 illustrating a progradational trend. The presence of numerous *Aucellina* sp. and of abundant
590 pyrite suggests reducing conditions, which represent the equivalent of one of the upper Aptian
591 anoxic events known in southeastern France (Kennedy et al., 2014 and references therein). This
592 sequence is correlated with the Lemgo Fm of Rey et al. (1988) and Witam (1998).

593 In Tamzergout, the Aptian–lower Albian succession is thicker than elsewhere, and the more
594 complete ammonite succession suggests that an additional sequence (12 m) is preserved below
595 the major discontinuity of the Aptian–Albian boundary (D 4', Fig. 8). If so, this would imply
596 on one hand that subsidence was higher in this area than in other areas, and on the other hand
597 that the overlying unconformity surface is strongly erosive, as this sequence is not recorded
598 elsewhere.



599

600 *Figure 9. East-West correlations of the Aptian–lower Albian sections in the central part of the*
 601 *Essaouira-Agadir Basin. D: dysaerobic facies. See Fig. 10 for caption, and Fig. 3 for explanation of I*
 602 *to 4, and I to IV.*

603 The **fifth sequence** (< 35 m) is well represented in all studied sections. It yielded numerous
 604 ammonites, which ensure an earliest Albian age (*L. tardefurcata* Zone). The lower sequence
 605 boundary (D 4, Figs. 5, and 8 to 10) is a typical S 4B surface at the base of a reworked bed,
 606 reflecting strong erosion. Among the reworked bioclasts in the basal sandy bed, the presence
 607 of corals (Addar), pectinids (Tamzergout), oysters (Tiskatine, Takoucht) or regular urchins (Ida
 608 w Shayq) suggests a shallow marine environment. Therefore, the occurrence of subaerial
 609 erosion related to a significant sea-level drop cannot be ruled out for this sequence boundary,
 610 which encompasses the Aptian–Albian boundary time-span. An emersion period during D 4 is
 611 supported by the fact that sequence 4 is locally deeply eroded, with its thickness varying
 612 between 30 m (Tamzergout) and 5 m (Anzate) in the South (Fig. 8), and between 4 m
 613 (Aoulkjdad) and 11 m (Taounerine) in the center of the basin (Fig. 9). The fifth sequence is
 614 mainly made of shaly marlstone, containing belemnites, ammonites and plicatulids, although
 615 oysters, brachiopods, pectinids and annelids may occur as well. This sequence is locally rich in
 616 buchidae bivalves (*Aucellina* sp.) (Takoucht, Aoulkjdad), especially in its upper part (Tinfoul,
 617 Tiskatine), suggesting dysaerobic conditions (e.g. Henderson, 2004).

618 Due to poor outcrop conditions, the identification of the sixth and seventh sequences are still
 619 preliminary. The ammonite content of the **sixth sequence** (< 20 m) indicates an early Albian
 620 age (late *L. tardefurcata* Zone and *D. mammillatum* Superzone p.p.). In all sections, the lower
 621 sequence boundary (D 5, Figs. 5, and 8 to 10) is a S 4B surface. Beside pelagic fauna, the strata
 622 overlying D 5 contains a molluscan fauna (brachiopods, pectinids, plicatulids) not as shallow

623 as those overlying D 4, and frequent phosphatized internal molds. Therefore, D 5 may
 624 correspond to a submarine erosion period. The fauna is dominated by belemnites, serpulids and
 625 plicatulids; some flat ammonites ("Beudanticeras beds") are present in the lower part, and
 626 *Aucellina* sp. and serpulids are quite abundant in some sections (Tiskatine, Aoulkjdad,
 627 Takoucht, Tamzergout). The latter indicate a clear dysaerobic environment, which may be an
 628 equivalent of the organic-rich deposits of the coeval "Niveau Paquier" of southeastern France
 629 (Kennedy et al., 2000). The top of the sequence is marked by the increase of sandy beds,
 630 suggesting the progradation of a coastal clastic system.

West **East**

CAPTION

I. Facies I: Distal outer ramp
 II, 1 Facies II or facies 1: Proximal outer ramp
 III, 2 Facies III or facies 2: Distal Middle ramp
 IV, 3 Facies IV or facies 3: Proximal middle ramp
 4 Facies 4: Inner ramp to intertidal
 D Dysaerobic facies

631
 632 *Figure 10. East-West correlations of the Aptian-lower Albian sections in the northern part of the*
 633 *Essaouira-Agadir Basin. D: dysaerobic facies. See Fig. 3 for explanation of 1 to 4, and I to IV.*

634
 635 The **seventh sequence** (< 30 m) has been identified only in the Tamzergout, Tiskatine,
 636 Aoulkjdad and Takoucht sections. Its poor ammonite content indicates an early Albian age (*D.*
 637 *mammillatum* Superzone p.p.). The lower discontinuity (D 6, Fig. 8 and 9) is an erosional
 638 surface (S 4B) overlain by a sandstone bed containing phosphate clasts. Sequence 7 consists of
 639 sandy/silty marls with abundant sandy limestone and sandstone beds. The fauna is similar to
 640 that of the sixth sequence (plicatulids, serpulids, belemnites, *Aucellina* sp., scarce large
 641 bivalves). In Tinfoul and Anzate, this sequence is probably present but has not been
 642 differentiated from the sixth sequence (Fig. 8). The thickness of the sequence and the amount
 643 of detrital quartz and sandstone beds seem to increase toward the North and East (Tinfoul,
 644 Aoulkjdad, Takoucht).

645 An **eighth sequence** is locally partly visible (Addar, Tiskatine, Aoulkjdad, Tamzergout). Its
 646 lower boundary (D 7, Figs. 5 and 7) is an S 4B surface. The sandstone bed overlying D 7
 647 contains wood remains, ostreids, frequent lithoclasts, and locally presents parallel laminae and
 648 Hummocky Cross Stratification, which suggest a very shallow depositional environment. These
 649 features suggest that D 7 may correspond to a subaerial erosion period. This interpretation is
 650 substantiated by common plant remains in the abundant sandstone beds of the underlying
 651 sequence 7, which suggest the proximity of emergent land. Scarce and little diversified

652 ammonites indicate an early Albian age. The rare faunal content comprises ammonites,
653 belemnites, plicatulids and serpulids in the sandstone beds, and *Aucellina* sp. in the sandy,
654 marly shales. Together with the apparent scarcity of bioturbation, this suggests ongoing dysoxic
655 conditions. The overlying shales are frequently covered. The fifth to eighth sequences constitute
656 the lower part of the Oued Tidzi Fm (Duffaud et al., 1966).

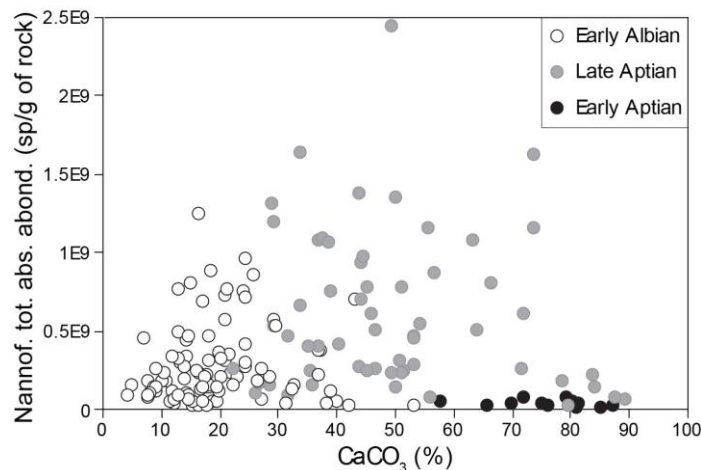
657 **V.2. Comparison with other areas**

658 Although the Aptian period has been extensively studied for paleoenvironmental and
659 paleoceanographic conditions (e.g. Sabatino et al., 2015, and references therein), relatively
660 few works are available on the sequence stratigraphy of this stage. A SB of latest Barremian
661 age (within the *Martellites sarrasini* Zone) has been identified in southern (Ruiz-Ortiz and
662 Castro, 1998) and northern Spain (Bover-Arnal et al., 2009), and in the Urgonian platform of
663 the Swiss and French Prealps (Arnaud et al., 1998; Clavel et al., 2013; Tendil et al., 2018),
664 which correlates with our D0. Some authors mentioned a first lower Aptian SB around the limit
665 between the *Deshayesites oylanensis* and *D. forbesi* ammonite zones (Bover-Arnal et al., 2009;
666 Martín-Martín et al., 2013; Tendil et al., 2018), and a second one between the *D. forbesi* and *D.*
667 *deshayesi* zones (Ruiz-Ortiz and Castro, 1998; Arnaud et al., 1998; Raddadi, 2004; see also
668 Embry et al., 2010). Because of common condensation and poor sedimentary record, none of
669 these discontinuities has been recognized confidently in the EAB, most probably due to the low
670 sea level globally recorded in earliest Aptian times (e.g. Haq, 2014). A third lower Aptian SB
671 has been dated as close to the *D. deshayesi-Dufrenoyia furcata* ammonite zones boundary
672 (Martín-Martín et al., 2013; H. Arnaud, pers. comm., 2014), which may be correlated with D1.
673 D2, dated as close to the early-late Aptian boundary (*D. furcata-Epicheloniceras martini* zones)
674 is probably coeval with the SB identified in Spain (Bover-Arnal et al., 2009; Martín-Martín et
675 al., 2013; Embry et al., 2010) and in south-eastern France (H. Arnaud, pers. comm., 2014; Pictet
676 et al., 2015). The SB identified in Spain within the *E. martini* and *Parahoplites melchioris* zones
677 (Ruiz-Ortiz and Castro, 1998; Bover-Arnal et al., 2009; Martín-Martín et al., 2013) has been
678 recognized neither in the EAB, nor in southern France (Raddadi, 2004; Clavel et al., 2013). The
679 D3 identified in the EAB is located within the *Acanthohoplites nolani* Zone, and therefore, is
680 correlatable with the SB identified in southern Spain (Ruiz-Ortiz and Castro, 1998), while D4'
681 seems to be correlatable with the SB identified in the late *Hypacanthoplites jacobi* Zone in
682 Spain (Ruiz-Ortiz and Castro, 1998; Bover-Arnal et al., 2009; Martín-Martín et al., 2013) and
683 Tunisia (Chihaoui et al., 2010; Latil, 2011; Hfaied et al., 2013). D4 of the EAB, the erosional
684 surface of which contains the Aptian–Albian boundary, is easily correlated with the base of the
685 Hameima Fm in Central Tunisia (Chiahoui et al., 2010; Latil, 2011) and with the base of the
686 Alb 1 sequence of Hfaied et al. (2014) in southern Tunisia, both marked by a sedimentary hiatus.
687 In Spain, it probably correlates with the Aptian–Albian boundary of Martín-Martín et al. (2013)
688 and with Sb7 of Ruiz and Castro (1998). As a consequence, and taking into account that poor
689 sedimentary record may have locally limited SB identification in the EAB, the good
690 chronological correlations with other regions of the Tethys suggest that sea-level variations
691 were the main factor controlling the sedimentary discontinuities in the EAB during Aptian–
692 early Albian times.

693 **V.3. Calcareous nannofossil primary productivity and carbonate production**

694 The nannofossil total absolute abundance depends on primary productivity in the water column,
695 preservation, and sedimentation rate. Significantly lower nannofossil total absolute abundances
696 are observed in Albian than in Aptian strata in samples with different preservation states (poor
697 to good; Fig. 7) and thus do not result from a poor preservation. The decrease in nannofossil
698 total abundance is associated with an increase in the relative abundance of high-fertility
699 nannofossils indicators, which seems contradictory. Indeed, both high nannofossil total
700 abundances and relative abundances of high-fertility taxa can be related to a high primary

701 productivity in marine surface waters. The Aptian lower parts of the sections are more
 702 condensed with respect to the lower Albian upper parts, and the change to higher sedimentation
 703 rates occurs above D4. Thus, the decrease in nannofossil total absolute abundances recorded in
 704 all sections through early Albian times may be explained by an increase in the sedimentation
 705 rate, with a dilution effect by the siliciclastic fraction. During the early Albian, enhanced
 706 relative abundances of high-fertility taxa suggest an increase in the nannofossil primary
 707 productivity.



708
 709 *Figure 11. Bivariate plot showing the relationship between CaCO₃ content and calcareous*
 710 *nannofossil absolute abundance for different time intervals, recognized in the Essaouira-Agadir basin.*
 711 *176 measurements from the Addar, Alma, Anzate, Ida w Shayq, Tinfoul and Tiskatine sections.*

Taxa	Surface-water fertility	Paleoceanography
<i>Biscutum constans</i>	high ^{1,2,3,4,5,6,7,8,9} high, but lower than <i>Z. erectus</i> ^{10,11,12}	
<i>B. ellipticum</i> *	high ² moderate to high ¹³	
<i>Biscutum</i> spp.**	moderate ¹⁴	
<i>Crucibiscutum salebrosum</i>		high latitude ^{15,16,17}
<i>Discorhabdus rotatorius</i>	high ^{4,5,18} moderate ¹³	
<i>Lithraphidites carniolensis</i>	moderate ^{4,5}	
<i>Nannoconus</i> spp.	low ^{9,18,19,20,21} low to moderate ²² , moderate ²³	warm waters ^{9,24} , deep-dweller ²¹
<i>Repagulum parvidentatum</i>		high latitude ^{17,25,26,27,28}
<i>Rhagodiscus angustus</i>		high latitude ²⁷
<i>Seribiscutum gaultensis</i>		high latitude ²⁹
<i>S. primitivum</i>		high latitude ^{1,2,3,16,17,27,28}
<i>Zeugrhabdodus erectus</i>	high ^{1,2,3,6,7,10}	
small <i>Zeugrhabdodus</i> (with major axis ≤ 5 μm)	high ^{7,8,11}	

**B. ellipticum* is considered as a morphotype of *B. constans* (Bornemann and Mutterlose, 2006)
 ***Biscutum* spp.: *B. constans* (abundant), *B. ellipticum* (common) (Linnert et al., 2010)

712
 713 *Table 2. Paleoecological significance of selected calcareous nannofossil taxa. 1. Roth (1981); 2. Roth*
 714 *and Bowdler (1981); 3. Roth and Krumbach (1986); 4. Erba (1987); 5. Premoli Silva et al. (1989); 6.*
 715 *Roth (1989); 7. Watkins (1989); 8. Williams and Bralower (1995); 9. Mutterlose and Kessels (2000);*
 716 *10. Erba (1992); 11. Erba et al. (1992); 12. Elson and Bralower (2005); 13. Giraud et al. (2003); 14.*
 717 *Linnert et al. (2010); 15. Mutterlose (1992a); 16. Mutterlose (1992b); 17. Street and Bown (2000);*
 718 *18. Coccioni et al. (1992); 19. Tappan (1980); 20. Busson and Noël (1991); 21. Erba (1994); 22.*
 719 *Pauly et al. (2012); 23. Scarparo Cunha and Shimabukuro (1997); 24. Mutterlose (1989); 25. Wise*
 720 *(1988); 26. Erba et al. (1989); 27. Crux (1991); 28. Watkins et al. (1996); 29. Lees (2002).*

721 In a carbonate ramp setting such as the EAB, carbonate production may result from benthic
 722 fauna and/or from pelagic organisms, such as calcareous nannofossils. We have investigated
 723 more in detail the relationship between nannofossil total abundance and calcium carbonate

724 content. When all data from the different sections are plotted, a correlation exists between these
725 two variables, but remains unclear, especially for high values of calcium carbonate content (>
726 70%) corresponding to Aptian samples (Fig. 11). If the latter values are not taken into account,
727 a low positive correlation ($r = 0.343$, with 162 values and $p < 0.0001$) is observed. This suggests
728 that on the EAB ramp, the carbonate fraction was partly produced by calcareous nannofossils,
729 especially in sediments with values of calcium carbonate content lower than 70%.

730 The carbonate production was lower for the early Albian deposits in comparison to the Aptian
731 deposits in the EAB. This is shown by a decrease in the carbonate content starting around D4
732 (Fig. 6), by a decrease in both semi-quantitative abundance and diversity of shallow marine
733 benthic fauna, and by a decrease in the relative abundances of the bigger calcareous nannofossil
734 calcifier such as *Nannoconus* spp (Fig. 6). The latter is considered as a deep dweller, which is
735 more abundant in marine paleoenvironments with prevailing oligotrophic sea-surface
736 conditions (Table 2).

737 In carbonate oligotrophic environments, the photic zone is supposed to be thicker than in
738 siliciclastic environments, leading deep dweller to develop. This explains that nannoconids 1)
739 are less present in the proximal, more siliciclastic section of Tinfoul with respect to the other
740 sections, and 2) are much more abundant in the upper Aptian carbonate-rich deposits
741 corresponding to low fertility surface waters, with respect to the more siliciclastic deposits that
742 prevailed during the early Albian. Nannoconids are also associated with warm marine
743 paleoenvironments (Table 2). Decrease in their relative abundance in the latest Aptian-early
744 Albian interval may indicate cooler sea-surface temperatures. As a matter of fact, the significant
745 increase in the relative abundance of cold water nannofossil taxa in the latest Aptian, and overall
746 in the earliest Albian, suggests that cooling occurred, but may be also due to connections with
747 higher latitudes, linked to the recorded sea-level rise. However, connections with higher
748 latitudes cannot explain the decrease in the relative abundance of warm water nannofossil taxa,
749 such as nannoconids. In most of the studied sections the maximum relative abundance of cold
750 water taxa is reached in the early *D. mammillatum* ammonite Superzone. Such sea-water
751 temperature cooling in the late Aptian and earliest Albian is consistent with previous studies in
752 other Tethyan areas (e.g. Bottini et al., 2015; Bodin et al., 2015), although other authors
753 advocated for an ongoing warm climate in parts of the Tethyan realm (see discussion in Föllmi,
754 2012).

755

756 **V.4. Dynamics of the EAB in Aptian–early Albian times**

757 **V.4.1. General statement**

758 Deposition during the Aptian–early Albian is marked in the EAB by an overall low energy
759 environment, as documented by the lack of oolites, coral reefs or grainstone textures.
760 Additionally, the abundance of pyrite in marls, together with the abundant buchidae, suggests
761 that bottom waters were little oxygenated in the middle to distal areas. Facies successions are
762 monotonous and lateral changes are quite gradual. These observations call for a very low-sloped,
763 even ramp topography. The lack of high-energy deposits is probably favoured by the
764 geographic location of the EAB on the western side of a continent. As a matter of fact, in the
765 northern hemisphere, storms are formed in intertropical latitudes and shift first toward the West,
766 due to the trade winds, and then to the North, because of the Coriolis deviation, thus affecting
767 the eastern or southern coasts of the continents. Since the EAB is located on the northwestern
768 margin of Africa, storms were probably scarce, thus favoring a low energy regime and possibly
769 water stratification. Coastal upwelling enhanced by the westward trade winds might have
770 favoured biological activity, resulting in little oxygenation of bottom water in the outer ramp
771 and organic-rich deposition shoreward.

772 On the other hand, during the late Aptian–early Albian interval, the faunal assemblages are
773 dominated by brachiopods, oysters, plicatulids, pectinids and other bivalves, as well as
774 serpulids, gastropods and irregular urchins. Conversely, they are almost devoid of oolites,
775 oncolites, stromatolites, corals, rudistids and algae. This suggests that, in spite of its
776 intertropical latitude (15 to 20° lat. N; e.g., Trabucho-Alexandre et al., 2011), the EAB behaved
777 as a temperate platform, at least during late Aptian and early Albian times.

778 The occurrence of phosphate- and glauconite-rich crusts or clasts suggests that the EAB was
779 submitted to cold, upwelling currents, as documented by Leckie (1984), Herrle et al. (2004),
780 Haydon et al. (2008) and Hofmann et al. (2008) along the Moroccan margin. This interpretation
781 is supported, on one hand by the abundance of glauconite and phosphate clasts in upper Aptian
782 to lower Albian deposits. On the other hand, the westernmost areas (Tamri, Assaka, Imsouane;
783 Fig. 1 and 9) exhibit very condensed sections, where 50 cm-thick, glauconite- and phosphate-
784 rich conglomerates contain ammonites of early Aptian to earliest Albian age. Such a
785 condensation may be attributed to significant, continuous upwelling currents affecting the
786 western edge of the ramp during Aptian to earliest Albian times.

787 **V.4.2. Comparison between Aptian and latest Aptian–early Albian environments**

788 Albian facies differ from the Aptian ones by the abundance of clastic input. A high carbonate
789 production is favoured by a large photic zone, few terrigenous influx, warm sea-surface
790 conditions and slow rise of sea level. Albian facies differ from the Aptian ones by the abundance
791 of detrital input. Aptian deposits comprise marls and limestones, with few, fine grained detrital
792 quartz. Conversely, Albian sedimentation is marked by silty marls and shales, and sandstones.
793 This provoked a change in the overall faunal content. As a matter of fact, pectinids and irregular
794 sea urchins, common in the Aptian beds, are much scarcer in lower Albian deposits, whereas
795 oysters and plicatulids are much more abundant in the latter. In the same way, scarce corals are
796 present in the Aptian succession but are totally absent in the lower Albian series. Although the
797 development of oysters from Albian times onward is a widespread feature that may be related
798 to a global sea-level rise (Dhondt et al., 1996), this suggests also that the lower Albian
799 environment is marked by more important terrigenous sediment supply (local occurrence of
800 plant fragments), and associated nutrients input to the basin, which led to both a reduction of
801 the photic zone depth, and a change from oligotrophic to mesotrophic conditions, illustrated
802 both by increasing calcareous primary productivity and the faunal change. Increasing
803 terrigenous supply was probably caused by enhanced runoff from the emergent continents
804 during more humid climatic conditions. However, the highest nannofossil primary productivity
805 conditions are recorded above D4 (*L. tardefurcata* and early *D. mammillatum* ammonite Zones),
806 which corresponds to a period of sea-level rise. Therefore, increasing nutrient content could
807 also be due to upwelling encroaching the platform during sea-level rise and high sea-level
808 periods.

809 The average deposition depth seems to have been higher in the early Albian than during the
810 Aptian. During the latter period, the deposition depth varied between 0 meters (S 1) and little
811 below the lower limit of the euphotic zone (F 1), whereas in the early Albian, deposition depth
812 varied from the fair weather wave base (F IV), to largely below the euphotic zone (lack of
813 benthic macrofauna in F I). However, this qualitative assessment may be exaggerated, as the
814 more important detrital sediment supply during the early Albian might have reduced the
815 thickness of the photic zone because of repeated clay input into the basin. Therefore, we cannot
816 rule out that facies F II and F III may have been deposited in environments equivalent to, or
817 slightly shallower than, facies F 1 and F 2, respectively.

818 The average energy level that prevailed during deposition of the lower Albian succession was
819 higher than during the Aptian, as shown by the occurrence in the lower Albian succession of

820 erosional surfaces, dolomitic sandstone beds and current structures in the latter. Since many of
821 these beds overlie erosional surfaces and thus correspond to drops in sea level, this suggests
822 that these high energy deposits were sedimented in an environment shallower than the storm
823 wave base, or even shallower than the fair weather wave base. This supports the fact that the
824 average deposition depth remained moderate, even during the early Albian.

825 Finally, the F D facies are restricted to the lower Albian succession, which suggests that the
826 EAB ramp was more oxygen-depleted at that time, than during the Aptian. Two causes may be
827 invoked. On one hand, the O₂ depleted zone may have been too deep to reach the Moroccan
828 ramp during the Aptian, whereas, the higher deposition depth during the early Albian allowed
829 the O₂ depleted zone to reach and impinge upon the EAB. On the other hand, the influence of
830 upwelling currents may have favoured the marine life in the outer zones of the ramp, consuming
831 a part of the available oxygen through biological activity and organic matter degradation, thus
832 favoring the extension of the O₂ depleted zone onto the EAB ramp (e.g. Erbacher et al., 1996;
833 Haydon et al., 2008). One of these O₂ depleted deposits may have been coeval with the OAE1b,
834 since it occurred in Tamzergout during the *L. tardefurcata* ammonite Zone (Peybernès et al.,
835 2013), and has been recognized in Takoucht at the same level (Fig. 5 and 10). There, TOC
836 measurements indicate fluctuations around 1% TOC, but due to the lack of other TOC analysis
837 in other intervals, no comparison can be made.

838

839 **V.5. Paleogeographic and tectonic evolution**

840 During latest Barremian to earliest late Aptian times (Sequences 1 and 2, *M. sarasini* to *E.*
841 *martini* p.p. ammonite Zones), the western, southern and eastern areas of the basin are marked
842 by repeated emersions (numerous karstic and epikarstic cavities), which likely produced
843 erosions of part of the previous deposits. As a consequence, S1 and S2 in these areas are absent
844 or extremely reduced. In many sections, however, the occurrence of ammonites shows that
845 marine sedimentation sporadically occurred. Significant carbonate sedimentation only took
846 place in the central part of the EAB (Fig. 12A). This pattern seems inherited from the latest
847 Barremian paleogeography, during which only in the central part of the EAB accumulated a
848 significant thickness of fine-grained marine sandstone (≈ 5 m), while the western and southern
849 part of the area were submitted to subaerial to submarine condensation (Jaillard et al., 2019)
850 It suggests that the western and southern parts of the EAB were slightly uplifted with respect
851 to the central part around the Barremian–Aptian boundary.

852 During late Aptian and early Albian times (Sequences 3 to 5), an increase of the depositional
853 depth is recorded by the eastward retrogradation of the sedimentary facies. Shallow marine
854 carbonates were dominant during Sequence 3 and almost disappeared during Sequence 5,
855 whereas outer ramp deposits were absent during Sequence 3 and became predominant during
856 Sequence 5 (Figs. 12B to 12D). Meanwhile, the southern coastal part of the area (Asaka, Tamri)
857 recorded a submarine condensation (glauconites, phosphate) likely related to upwelling
858 currents, assumed to be active offshore the Moroccan margin in Aptian–Albian times (Herrle
859 et al., 2004; Haydon et al., 2008). Deposition resumed during earliest Albian times, since
860 Sequence 5 is recorded in all studied sections. Note that the Tamzergout area shows a quite
861 localized thickness anomaly, which suggests an anomalous subsidence regime.

862 During the early Albian, the studied outcrops are insufficient to allow detailed facies mapping.
863 However, Sequences 6 and 7 (late *L. tardefurcata* and early *D. mamillatum* Zones) are
864 dominated by outer ramp facies in all areas, including in the southwestern part of the area where
865 the long-lasting submarine condensation ended, and by more homogeneous thicknesses. The
866 thickness anomaly of the Tamzergout area seems to have disappeared.

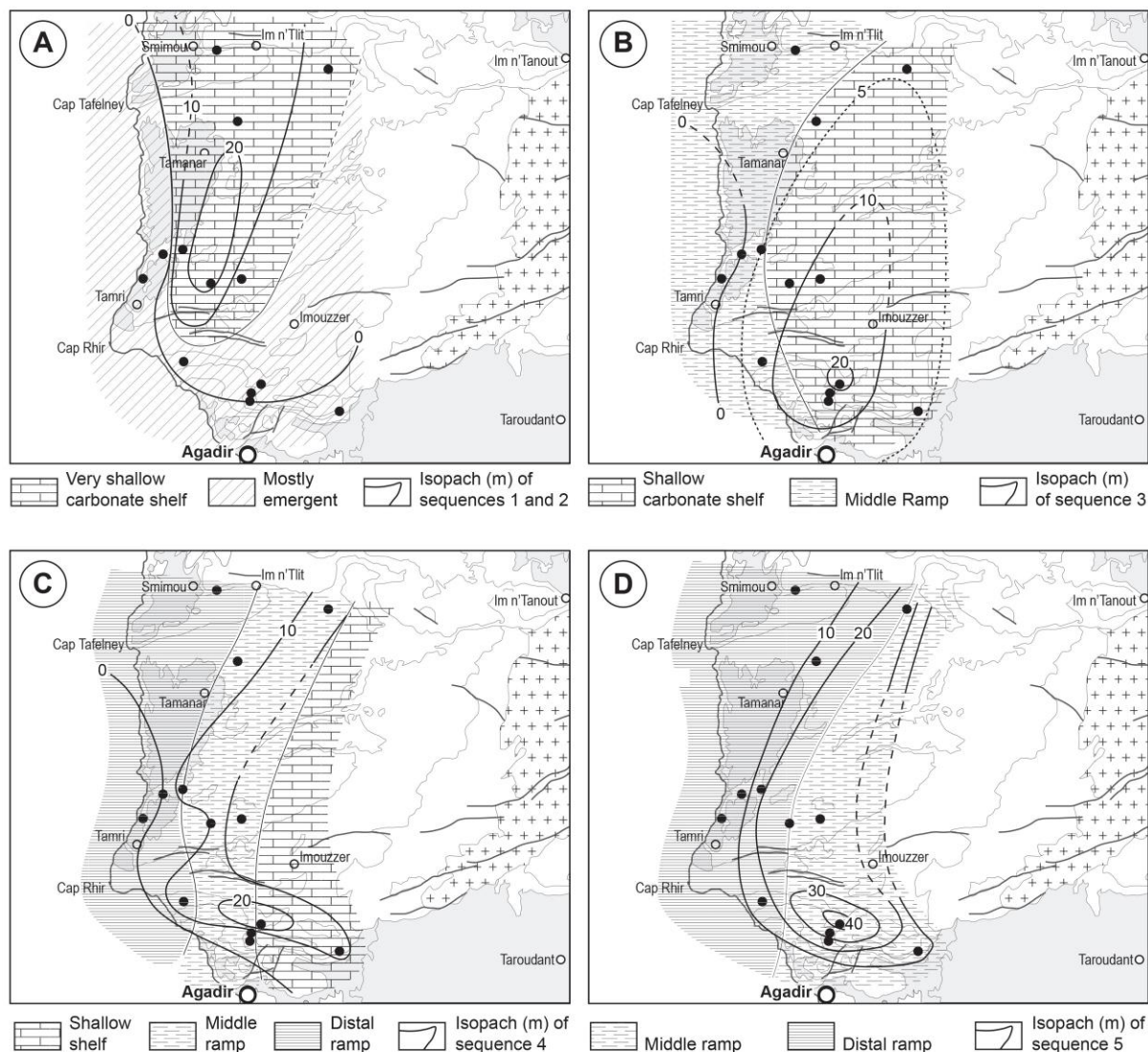


Figure 12. Paleogeographic and isopach maps of the study area. A. Sequences 1 and 2 (latest Barremian-Early Aptian); B. Sequence 3 (Early Late Aptian); C. Sequence 4 (latest Aptian); D. Sequence 5 (earliest Albian).

867
868
869
870
871

872 As a whole, the paleotopography inherited from the Upper Barremian tectonic event (i.e. uplift
873 of the southern and western areas; Jaillard et al., 2019) seems to be progressively leveled by the
874 lower Aptian accumulation. However, subsidence anomalies are recorded around the present-
875 day Amsittene and Imouzzzer anticlines, which are presently underlain by evaporitic diapirs
876 (Mrhidek et al., 2000; Tari and Jabour, 2013). To the north, the Amsittene anticline and its
877 surroundings are marked by a low subsidence regime (Aptian sequences are less than 10 m
878 thick), and to the south, the Imouzzzer anticline is first uplifted (Sequences 1 and 2), and then
879 presents an anomalously high subsidence in the Tamzergout section. This localized subsidence
880 anomaly is most likely related to the presence of underlying evaporites, and may be due either
881 to the formation of a rim-syncline or mini-basin located in the vicinity of a rising diapir (e.g.
882 Gilles and Rowan, 2012; Brandes et al., 2012), or to a collapse structure above a karstic system
883 caved in evaporites (e.g. Belderson et al., 1978; Gutiérrez et al., 2008). In the latter
884 interpretation, the occurrence of repeated emersions may have favoured dissolution of evaporite,
885 but the radial or concentric normal faults, commonly associated with these structures (Stewart,
886 2006), were not observed in the field, neither at small-scale, nor at large-scale. In the former

887 interpretation, the absence of normal faults is frequent in rim-syncline structures, which show
888 locally a ring-shaped morphology or are surrounded by uplifted areas above the rising diapir.
889 These features seem consistent with our data, but more geological observations and surveying
890 are needed to choose between these two interpretations.

891

892 VI. CONCLUSIONS

893 Our detailed study of the Aptian–lower Albian succession of the EAB allowed to define a
894 biostratigraphic framework, correlated with the standard ammonite zonation of Europe. In this
895 scheme, lowermost Aptian deposits are lacking, lower Aptian strata are poorly represented, and
896 the Aptian–Albian boundary is included within a hiatus marked by a major sedimentary
897 diecontinuity.

898 Careful analysis of sedimentary facies and surfaces made possible to decipher the sedimentary
899 evolution of the EAB during Aptian–early Albian times, and to subdivide this interval into eight
900 depositional sequences. The latter can be correlated with coeval sequences identified in other
901 Tethyan areas, thus suggesting that they were mainly controlled by eustatic variations. In this
902 context, the lack of the lowermost Aptian sequences is most probably related to the significant
903 sea-level fall recorded at that time (Haq, 2014).

904 As a whole, Aptian–lower Albian sediments of the EAB were deposited on a low energy ramp
905 that evolved from a carbonate to a mixed carbonate-clastic system. This evolution occurred
906 progressively in Late Aptian times and was associated with an increase of sandy and shaly
907 deposits, with a change from oligotrophic to mesotrophic faunal and nannofossil assemblages,
908 and with an increase of cold water nannofossil taxa indicating a cooling of sea-surface
909 temperatures. Deposition depth seems to be slightly higher in the early Albian than during the
910 Aptian, consistent with the eustatic sea-level rise recorded at that time. The more energetic
911 environment displayed by lower Albian deposits, together with the occurrence of dysaerobic
912 deposits and the abundance of phosphate and glauconite, suggest that upwelling currents were
913 significant in Aptian to early Albian times.

914 The overall sea-level rise in the late Aptian and early Albian is illustrated by the evolving facies
915 distribution on paleogeographic reconstructions. Furthermore, the latter evidence subsidence
916 anomalies around the present-day anticlines cored by evaporites, thus suggesting the play of
917 mild halokinetic movements during Aptian–early Albian times.

918

919 **Acknowledgements** : Most of the data presented here result from (1) a collaborative program carried
920 out between the universities of Grenoble, Agadir, Lyon and Marrakech, funded by the Ministries of
921 foreign affairs from France and Morocco (PHC project n° 031/STU/13), which resulted in the
922 achievement of a university thesis (Hassanein, 2016). We benefited from a financial support by the
923 french Institut de Recherche pour le Développement (IRD) to W.H.K. (PhD grant) and E.J. (field trips),
924 and from an annual financial support by the ISTERre, Grenoble, and Terre Planètes Environnement, Lyon,
925 laboratories, and by the OSUG@2020 Labex program of the Observatoire des Sciences de l'Univers de
926 Grenoble. We warmly thank M. Aoutem (Agadir) for his help in field work, F. Baudin (Sorbonne
927 Université) for TOC analysis and interpretation, and J.-L. Latil for fruitful paleontological and
928 biostratigraphic discussions. M. Bernet (Grenoble) is thanked for revising the English text. Sincere
929 thanks are due to Serge Ferry and an anonymous reviewer for their fair and constructive reviews.

930

931 References

932 Al Yacoubi, L., Bouchaou, L., Jaillard, E., Masrour, M., Ait Brahim, Y., El Mouden, A., Schneider, J., Reichert,
933 B., 2017. Impact of rock-water interactions and recharge on water resources quality of the Agadir-Essaouira
934 Basin, Southwestern Morocco. *Arabian Journal of Geosciences* 10: 169, DOI 10.1007/s12517-017-2968-2.

- 935 Algouti, A., Algouti, A., Taj-Eddine, K., 1999. Le Sénonien du Haut Atlas occidental, Maroc : sédimentologie,
936 analyse séquentielle et paléogéographie. *Journal of African Earth Sciences* 29, 643-658.
- 937 Ambroggi, R., 1963. Etude géologique du versant méridional du Haut Atlas occidental et de la plaine du Souss.
938 Notes du Service géologique du Maroc 157, 322 pp.
- 939 Ambroggi, R., Breistroffer, M., 1959. Stratigraphie du Crétacé du Haut Atlas Occidental (Sud marocain).
940 Congreso geológico Internacional, Mexico 1956, sesión XX, n° 157, 33-40.
- 941 Andreu, B., 1989. Le Crétacé moyen de la transversale Agadir-Nador (Maroc) : précisions stratigraphiques et
942 sédimentologiques. *Cretaceous Research* 10, 49-80.
- 943 Arnaud, H., Arnaud-Vanneau, A., Blanc-Alétru, M.-C., Adatte, T., Argot, M., Delanoy, G., Thieuloy, J.-P.,
944 Vermeulen, J., Virgone, A., Virlouvét, B., Wermeille, S., 1998. Répartition stratigraphique des orbitolinidés
945 de la plate-forme urgonienne subalpine et jurassienne (SE de la France). *Géologie Alpine* 74, 3-89.
- 946 Aubry, M.P., Bord, D., Beaufort, L., Kahn, A., Boyd, S., 2005. Trends in size changes in the coccolithophorids,
947 calcareous nannoplankton, during the Mesozoic: a pilot study. *Micropaleontology* 51, 309-318.
- 948 Beaufort, L., 1991. Adaptation of the random settling method for quantitative studies of calcareous nannofossils.
949 *Micropaleontology* 37, 415-418.
- 950 Behar, F., Beaumont, V., De B. Penteadó, H.L. 2001. Rock-Eval 6 Technology: Performances and Developments.
951 *Oil & Gas Science and Technology* 56, 111-134.
- 952 Belderson, R.H., Kenyon, N.H., Stride, A.H., 1978. Local supmarine salt-karst formation on the Hellenic outer
953 Ridge, eastern Mediterranean. *Geology* 6, 716-720.
- 954 Bertotti, G., Gouiza, M., 2012. Post-rift vertical movements and horizontal deformations in the eastern margin of
955 the Central Atlantic: Middle Jurassic to Early Cretaceous evolution of Morocco. *International Journal of Earth
956 Sciences (Geol. Rundsch.)* 101, 2151-2165
- 957 Bodin, S., Meissner, P., Janssen, N.M.M., Steuber, T., Mutterlose, J., 2015. Large igneous provinces and organic
958 carbon burial: Controls on global temperature and continental weathering during the Early Cretaceous. *Global
959 and Planetary Change* 131, 238-253.
- 960 Bornemann, A., Mutterlose, J. 2006. Size analyses of the coccolith species *Biscutum constans* and *Watznaueria
961 barnesiae* from the Late Albian Niveau Breistroffer (SE France): taxonomic and palaeoecological implications.
962 *Geobios* 39, 599-615.
- 963 Bottini, C., Erba, E., Tiraboschi, D., Jenkyns, H.C., Schouten, S., Sinnighe Damsté, J.S., 2015. Climate variability
964 and ocean fertility during the Aptian stage. *Climate of the Past* 11, 383-402.
- 965 Bourgeois, Y., Ben Haj Ali, N., Razgallah, S., Tajeddine, K., 2002. Etude biostratigraphique du Crétacé inférieur
966 (Barrémien supérieur-Albien) du Haut Atlas occidental (Maroc), *Estudios Geológicos* 58, 105-112.
- 967 Bover-Arnal, T., Salas, R., Moreno-Bedmar, J.A., Bitzer, K., 2009. Sequence stratigraphy and architecture of a
968 late Early-Middle Aptian carbonate platform succession from the western Maestrat Basin (Iberian Chain,
969 Spain). *Sedimentary Geology* 219, 280-301.
- 970 Bown, P.R., Rutledge, D.C., Crux, J.A., Gallagher, L.T., 1998. Lower Cretaceous. In: Bown P.R. (Ed.), *Calcareous
971 nannofossil biostratigraphy*. British Micropalaeontological Society Publications Series. Chapman and
972 Hall/Kluwer Academic Publ., 86-102.
- 973 Bown, P.R., Young, J.R., 1998. Techniques. In: Bown P.R. (Ed.), *Calcareous nannofossil biostratigraphy*. British
974 Micropalaeontological Society Publications Series. Chapman and Hall/Kluwer Academic Publ., 16-28.
- 975 Brandes, C., Pollok, L., Schmidt, C., Wilde, V., Winseman, J., 2012. Basin modelling of a lignite-bearing rim
976 syncline: insights into rim-syncline evolution and salt diapirism in NW Germany. *Basin Research* 24, 699-716.
- 977 Brautigam, K., Fernández-Blanco, D., Klaver, J.M., 2009. Late Jurassic-Early Cretaceous horizontal tectonics
978 drives the Jbel Amsittene Anticline in the Haha Basin, Morocco. MSc. Thesis, Free University Amsterdam, 59
979 pp.
- 980 Brives, A., 1905. Contribution à l'étude géologique de l'Atlas marocain. *Bulletin de la Société géologique de
981 France* 5, 379-398.
- 982 Bulot, L.G., Latil, J-L., 2014. New insights on the genus *Nolaniceras* Casey, 1961 (Ammonoidea, Cretaceous) and
983 its consequences on the biostratigraphy of the Aptian Stage. *Proceedings of the Geologist's Association* 125,
984 227-232.
- 985 Burrollet, P.F., 1956. Contribution à l'étude stratigraphique de la Tunisie Centrale. *Annales des Mines et de la
986 Géologie* 18, 350 pp., 22 pl., Tunis.
- 987 Busson, G., Noël, D., 1991. Les nannoconidés indicateurs environnementaux des océans et mers épicontinentales
988 du Jurassique terminal et du Crétacé inférieur. *Oceanologica Acta* 14, 333-356.
- 989 Canérot, J., Cugny, P., Peybernès, B., Rahli, I., Rey, J., Thieuloy, J.-P., 1986. Comparative study of the Lower and
990 Mid-Cretaceous sequences on different maghrebien shelves and basins: Their place in the evolution of the
991 North African, Atlantic and Neotethysian margins. *Palaeogeography, Palaeoclimatology, Palaeoecology* 55,
992 213-232.

- 993 Chihaoui, A., Jaillard, E., Latil, J.-L., Susperregui, A.-S., Touri, J., Ouali, J., 2010. Stratigraphy of the Hameima
994 and Lower Fahdene formations in the Tadjerouine area (Northern Tunisia). *Journal of African Earth Sciences*
995 58, 387-399.
- 996 Clavel, B., Conrad, M.-A., Busnardo, R., Charollais, J., Granier, B., 2013. Mapping the rise and demise of
997 Urgonian platforms (Late Hauterivian - Early Aptian) in southeastern France and the Swiss Jura. *Cretaceous*
998 *Research* 39, 29-46.
- 999 Coccioni, R., Erba, E., Premoli Silva, I., 1992. Barremian-Aptian calcareous plankton biostratigraphy from the
1000 Gorgo a Cerbara section (Marche, Central Italy) and implication for planktonic evolution. *Cret. Res.* 13, 517-
1001 537.
- 1002 Crux, J.A., 1991. Albian calcareous nannofossils from the Gault Clay of Munday's Hill (Bedfordshire, England).
1003 *Journal of Micropalaeontology* 10, 203-221.
- 1004 Davison, I., Davy, P., 2010. Salt tectonics in the Cap Boudjour Area, Aaiun basin, NW Africa. *Marine and*
1005 *Petroleum Geology* 27, 435-441.
- 1006 De la Mora, A., Olóriz, F., González-Arreola, C., 2000. « Autochthonous » bivalve assemblages and
1007 palaeoecological interpretation in the Upper Jurassic-Lower Cretaceous La Caja Formation from the Cañón de
1008 San Matías (Zacatecas, México). *C. R. Acad. Sci. Paris, Earth and Planetary Sciences*, 331, 741-747.
- 1009 Dellisanti, F., Pini, G.A., Baudin, F., 2010. Use of Tmax as a thermal maturity indicator in orogenic successions
1010 and comparison with clay mineral evolution. *Clay minerals* 45, 115-146.
- 1011 Dhondt, A.V., Malchus, N., Boumaza, L., Jaillard, E., 1999. Cretaceous oysters from North Africa; origin and
1012 distribution. *Bulletin de la Société géologique de France* 170, 67-76.
- 1013 Duffaud, F., Brun, L., Plauchut, B., 1966. Le bassin du Sud-Ouest marocain. In: D. Reyre, (Ed.), Bassins
1014 sédimentaires du Littoral africain, 1^{ère} partie. Frimin Didot Publ., Paris, 5-12.
- 1015 Eleson, J.W., Bralower, T.J., 2005. Evidence of changes in surface water temperature and productivity at the
1016 Cenomanian/Turonian Boundary. *Micropaleontology* 51, 319-332.
- 1017 Embry, J.-C., Vennin, E., Van Buchem, F.S.P., Schroeder, R., Pierre, C., Aurell, M., 2010. Sequence stratigraphy
1018 and carbon isotope stratigraphy of an Aptian mixed carbonate-siliciclastic platform to basin transition (Galve
1019 sub-basin, NE Spain). *Geological Society, London, Special Publication* 329, 113-143.
- 1020 Erba, E., 1987. Mid-Cretaceous cyclic pelagic facies from the Umbrian-Marchean Basin: What do calcareous
1021 nannofossils suggest? *Int. Nannoplankton Assoc. Newsletter* 9, 52-53.
- 1022 Erba, E., 1992. Middle Cretaceous calcareous nannofossils from the western Pacific (Leg 129): evidence for
1023 paleoequatorial crossings. In: Larson, R.L., Lancelot, Y. et al. (Eds). *Proceedings of the Ocean Drilling*
1024 *Program, Scientific Results* 129, 189-201.
- 1025 Erba, E., 1994. Nannofossils and superplumes: the early Aptian "nannoconid crisis". *Paleoceanography* 9, 483-
1026 501.
- 1027 Erba, E., Guasti, G., Castradori, D. 1989. Calcareous nannofossils record fertility and temperature cycles: Evidence
1028 from the Albian Gault Clay Formation. *INA Newslett.* 11, 57-58.
- 1029 Erba, E., Castradori, D., Guasti, G., Ripepe, M., 1992. Calcareous nannofossils and Milankovitch cycles: the
1030 example of the Albian Gault Clay Formation (southern England). *Palaeogeography, Palaeoclimatology,*
1031 *Palaeoecology* 93, 47-69.
- 1032 Espitalié, J., Deroo, G., Marquis, F., 1985/1986. La pyrolyse Rock-Eval et ses applications. *Revue de l'Institut*
1033 *Français du Pétrole* 40, 563-579, 775-784; 41, 73-89.
- 1034 Ettachfani, E.M., Souhleb, A., Andreu, B., Caron, M., 2005. La limite Cénomanién-Turonien dans le Haut Atlas
1035 central, Maroc. *Geobios* 38, 57-68.
- 1036 Föllmi, K., 2012. Early Cretaceous life, climate and anoxia. *Cretaceous Research* 35, 230-357.
- 1037 Frizon de Lamotte, D., Saint Bezar, B., Bracène, R., 2000. The two main steps of the Atlas building and
1038 geodynamics of the western Mediterranean. *Tectonics* 19, 740-761.
- 1039 Frizon de Lamotte, D., Zizi, M., Missenard, Y., Hafid, M., El Azzouzi, M., Maury, R.C., Charrière, A., Taki, Z.,
1040 Benammi, M., Micard, A., 2008. The Atlas System. In: Michard, A. et al., (Eds), *Continental Evolution: The*
1041 *Geology of Morocco. Lecture Notes in Earth Sciences* 116, 133-202.
- 1042 Frizon de Lamotte, D., Raulin, C., Mouchot, N., Wrobel-Daveau, J.-C., Blanpied, C., Ringenbach, J.-C., 2011.
1043 The southernmost margin of the Tethys realm during the Mesozoic and Cenozoic: Initial geometry and timing
1044 of the inversion processes. *Tectonics* 30, TC3002, doi:10.1029/2010TC002691.
- 1045 Geisen, M., Bollmann, J., Herrle, J.O., Mutterlose, J., Young, J.R., 1999. Calibration of the random settling
1046 technique for calculation of absolute abundances of calcareous nannoplankton. *Micropaleontology* 45, 437-
1047 442.
- 1048 Gentil, L., 1905. Observations géologiques dans le sud marocain. *Bulletin de la Société géologique de France* 5,
1049 521-523.
- 1050 Giles, K.A., Rowan, M.G., 2012. Concepts in halokinetic-sequence deformation and stratigraphy. *Geological*
1051 *Society, London, Special Publication* 363, 7-31.

1052 Giorgioni, M., Keller, C.E., Weissert, H., Hochuli, P.A., Bernasconi, S.M., 2015. Black shales – from coolhouse
1053 to greenhouse (early Aptian). *Cretaceous Research* 56, 716-731.

1054 Giraud, F., Olivero, D., Baudin, F., Reboulet, S., Pittet, B., Proux, O., 2003. Minor changes in surface water
1055 fertility across the Oceanic Anoxic Event 1d (latest Albian, SE France) evidenced by calcareous nannofossils.
1056 *International Journal of Earth Sciences* 92, 267-284.

1057 Guiraud, R., Bosworth, W., 1997. Senonian inversion and rejuvenation of rifting in Africa and Arabia: synthesis
1058 and implications to plate-scale tectonics. *Tectonophysics* 282, 39-82.

1059 Gutiérrez, F., Calaforra, J.M., Cardona, F., Ortí, F., Durán, J.J., Garay, P., 2008. Geological and environmental
1060 implications of the evaporite karst in Spain. *Environmental Geology* 53, 951-965.

1061 Hafid, M., Ait Salem, A., Bally, A.W., 2000. The western termination of the Jebilet-High Atlas system (offshore
1062 Essaouira Basin, Morocco). *Marine and Petroleum Geology* 17, 431-443.

1063 Hafid, M., Tari, G., Bouhadioui, D., El Moussaid, I., Ait Salem, A., Nahim, M., Dakki, M., 2008. Atlantic Basins.
1064 In: Michard, A. et al., (Eds), *Continental Evolution: the Geology of Morocco*. Lecture Notes in Earth Sciences
1065 116, 303-329.

1066 Haq, B.U., 2014. Cretaceous eustasy revisited. *Global and Planetary Change* 113, 44–58.

1067 Hassanein, W., 2016. The Aptian–Albian transgression in the Agadir-Essaouira Basin, Western Morocco. PhD
1068 Thesis, university Grenoble Alpes, 308 pp.

1069 Haydon, M., Adatte, T., Keller, G., Bartels, D., Föllmi, K.B., Steinmann, P., Berner, Z., Chellai, E.H., 2008.
1070 Organic deposition and phosphorus accumulation during Oceanic Anoxic Event 2 in Triffaya, Morocco.
1071 *Cretaceous Research* 29, 1008-1023.

1072 Henderson, R.A., 2004. A Mid-Cretaceous association of shell beds and organic-rich shale: Bivalve exploitation
1073 of a nutrient-rich, anoxic sea-floor environment. *Palaios* 19, 156-169.

1074 Herrle, J.O., Kössler, P., Friedrich, O., Erlenkeuser, H., Hemleben, C., 2004. High-resolution carbon isotope
1075 records of the Aptian to Lower Albian from SE France and the Mazagan Plateau (DSDP Site 545): a
1076 stratigraphic tool for paleoceanographic and paleobiologic reconstruction. *Earth and Planetary Science Letters*
1077 218, 149-161.

1078 Hfaied, R., Arnaud-Vanneau, A., Godet, A., Arnaud, H., Zghal, I., Ouali, J., Latil, J.-L., Jallali, H., 2013.
1079 Biostratigraphy, palaeoenvironments and sequence stratigraphy of the Aptian sedimentary succession at Jebel
1080 Bir Oum Ali (Northern Chain of Chotts, South Tunisia): Comparison with contemporaneous Tethyan series.
1081 *Cretaceous Research* 46, 177-207.

1082 Hofmann, P., Stüsser, I., Wagner, T., Schouten, S., Sinninghe Damsté, J.S., 2008. Climate-ocean coupling off
1083 North-West Africa during the Lower Albian: The Oceanic Anoxic Event 1b. *Palaeogeography, Palaeoclimatology, Palaeoecology*
1084 262, 157-165.

1085 Jaillard, E., Al Yacoubi, L., Reboulet, S., Robert, E., Masrour, M., Bouchaou, L., Giraud, F., El Hariri, K., 2019.
1086 Late Barremian eustasy and tectonism in the western High Atlas (Essaouira-Agadir Basin), Morocco.
1087 *Cretaceous Research* 93, 225-244.

1088 Jati, M., Grosheny, D., Ferry, S., Masrour, M., Aoutem, M., Içame, N., Gauthier-Lafaye, F., Desmares, D., 2010.
1089 The Cenomanian-Turonian boundary event on the Moroccan Atlantic margin (Agadir basin): Stable isotope
1090 and sequence stratigraphy. *Palaeogeography, Palaeoclimatology, Palaeoecology* 296, 151-164.

1091 Kennedy, W.J., Gale, A.S., Bown, P.R., Caron, M., Davey, R.J., Gröcke, D., Wray, D.S., 2000. Integrated
1092 stratigraphy across the Aptian-Albian boundary in the Marnes Bleues, at the Col de Pré-Guittard, Arnayon
1093 (Drôme), and at Tartonne (Alpes-de-Haute-Provence), France: a candidate Global Boundary Stratotype Section
1094 and Boundary Point for the base of the Albian Stage. *Cretaceous Research* 21, 591-720.

1095 Kennedy, W.J., Gale, A.S., Huber, B.T., Petrizzo, M.R., Bown, P., Barchetta, A., Jenkyns, H.C., 2014. Integrated
1096 stratigraphy across the Aptian/Albian boundary at Col de Pré-Guittard (southeast France): A candidate Global
1097 Boundary Stratotype Section. *Cretaceous Research* 51, 248-259.

1098 Kilian, W., Gentil, L., 1906. Découverte de deux horizons crétacés remarquables au Maroc. *Comptes rendus*
1099 *sommaire de l'Académie des Sciences de Paris* 142, 603-605.

1100 Kilian, W., Gentil, L., 1907. Sur les terrains crétacés de l'Atlas Occidental marocain. *Comptes rendus sommaire*
1101 *de l'Académie des Sciences de Paris* 144, 49-51.

1102 Klingelhoefer, F., Biari, Y., Sahabi, M., Aslamian, D., Schnabel, M., Matias, L., Benabdellouahed, M., Funck,
1103 T., Gutscher, M.-A., Reichert, C., Austin, J.A., 2016. Crustal structure variations along the NW-African
1104 continental margin: A comparison of new and existing models from wide-angle and reflection seismic data.
1105 *Tectonophysics* 674, 227-252.

1106 Kuroda, J., Tanimizu, M., Hori, R.S., Suzuki, K., Ogawa, N.O., Tejada, M., Coffin, M.F., Coccioni, R., Erba, E.,
1107 Ohkouchi, N., 2011. Lead isotopic record of Barremian–Aptian marine sediments: Implications for large
1108 igneous provinces and the Aptian climatic crisis. *Earth and Planetary Science Letters* 307, 126–134.

1109 Latil, J.-L., 2011. Lower Albian ammonites from Central Tunisia and adjacent areas of Algeria. *Revue de*
1110 *Paléobiologie* 30, 321-429.

- 1111 Leckie, R.M., 1984. Mid-Cretaceous planktonic foraminiferal biostratigraphy off Central Morocco, Deep Sea
1112 Drilling Project Leg 79, Sites 545 and 547. In: Hinz, K., Winterer, E.L., et al., Initial Reports DSDP 79, 579-
1113 620, Washington (U.S. Govt. Printing Office).
- 1114 Lees, J.A. 2002. Calcareous nannofossil biogeography illustrates palaeoclimate change in the Late Cretaceous
1115 Indian Ocean. *Cretaceous Research* 23, 537-634.
- 1116 Lemoine, P., 1905. Mission dans le Maroc occidental, Automne 1904, rapport au Comité du Maroc. Comité du
1117 Maroc (Paris), p. 223.
- 1118 Linnert, C., Mutterlose, J., Erbacher, J., 2010. Calcareous nannofossils of the Cenomanian-Turonian boundary
1119 interval from the Boreal Realm (Wunstorf, northwest Germany). *Marine Micropaleontology* 74, 38-58.
- 1120 Luber, T.L., Bulot, L.G., Redfern, J., Frau, C., Arantegui, A., Masrour, M., 2017. A revised ammonoid
1121 biostratigraphy for the Aptian of NW Africa: Essaouira-Agadir Basin. *Cretaceous Research* 79, 12-34.
- 1122 Luber, T.L., Bulot, L.G., Redfern, J., Nahim, M., Jeremiah, J., Simmons, M., Bodin, S., Frau, C., Bidgood, M.,
1123 Masrour, M., 2019. A revised chronostratigraphic framework for the Aptian of the Essaouira-Agadir Basin, a
1124 candidate type section for the NW African Atlantic Margin. *Cretaceous Research* 93, 292-317.
- 1125 Martín-Martín, J.D., Gomez-Rivas, E., Bover-Arnal, T., Travé, A., Salas, R., Moreno-Bedmar, J.A., Tomás, S.,
1126 Corbella, M., Teixell, A., Vergès, J., Stafford, S.L., 2013. The Upper Aptian to Lower Albian syn-rift carbonate
1127 succession of the southern Maestrat Basin (Spain): Facies architecture and faultcontrolled stratabound
1128 dolostones. *Cretaceous Research* 41, 217-236.
- 1129 Masrour, M., Aoutem, M., Atrops, F., 2004. Succession des peuplements d'échinides du Crétacé inférieur dans le
1130 Haut Atlas atlantique (Maroc) ; révision systématique et intérêt stratigraphique. *Geobios* 37, 595-617.
- 1131 Moulin, M., Aslanian, D., Unternehr, P., 2010. A new starting point for the South and Equatorial Atlantic Ocean.
1132 *Earth-Science Reviews* 98, 1-37.
- 1133 Mridekh, A., Toto, E.A., Hafid, M., El Ouataoui, A., 2000. Structure sismique de la plate-forme Atlantique au
1134 large d'Agadir (Maroc sud-occidental). C. R. Académie des Sciences, Paris, Earth and Planet Sciences,
1135 Géodynamique 331, 387-392.
- 1136 Müller, G., Gastner, M., 1971. The "Karbonat-Bombe", a simple device for the determination of the carbonate
1137 content in sediments, soils and other materials. *Neues Jahrbuch für Mineralogie - Monatshefte* 10, 466-469.
- 1138 Mutterlose, J., 1989. Temperature-controlled migration of calcareous nannofloras in the north-west European
1139 Aptian. In: Crux, J.A., van Heck, S.E. (Eds.), *Nannofossils and Their Applications*, 122-142, Ellis Horwood,
1140 Chichester.
- 1141 Mutterlose, J., 1992a. Lower Cretaceous nannofossil biostratigraphy off northwestern Australia (Leg 123). In:
1142 Gradstein, F.M., Ludden, J.N. (Eds.). *Proceedings of the Ocean Drilling Program. Scientific Results* 123, 343-
1143 368.
- 1144 Mutterlose, J., 1992b. Biostratigraphy and palaeobiogeography of Early Cretaceous calcareous nannofossils.
1145 *Cretaceous Research* 13, 167-189.
- 1146 Mutterlose, J., Kessels, K., 2000. Early Cretaceous calcareous nannofossils from high latitudes: implications for
1147 palaeobiogeography and palaeoclimate. *Palaeogeography, Palaeoclimatology, Palaeoecology* 160, 347-372.
- 1148 Pauly, S., Mutterlose, J., Alsen, P., 2012. Lower Cretaceous (upper Ryazanian-Hauterivian) chronostratigraphy of
1149 high latitudes (North-Esot Greenland). *Cretaceous Research* 34, 308-326.
- 1150 Perch-Nielsen, K., 1985. Mesozoic calcareous nannofossils. In: Bolli, H.M., Saunders, J.B., Perch-Nielsen, K.
1151 (Eds.): *Plankton Stratigraphy*, 329-426. Cambridge University Press.
- 1152 Peybernès, C., Giraud, F., Jaillard, E., Robert, E., Masrour, M., Aoutem, M., Içame, N., 2013. Calcareous
1153 nannofossil productivity and carbonate production on the southern tethyan margin (Morocco) during the Late
1154 Aptian-Early Albian : paleoclimatic implications. *Cretaceous Research* 39, 149-169.
- 1155 Pictet, A., Delanoy, G., Adatte, T., Spangenberg, J.E., Beaudouin, C., Boselli, P., Boselli, M., Kindler, P., Föllmi,
1156 K.B., 2015. Three successive phases of platform demise during the early Aptian and their association with the
1157 oceanic anoxic Selli episode (Ardèche, France). *Palaeogeography, Palaeoclimatology, Palaeoecology* 418,
1158 101-125.
- 1159 Premoli Silva, I., Erba, E., Tornaghi, M.E. 1989. Paleoenvironmental signals and changes in surface fertility in
1160 Mid Cretaceous Corg-rich pelagic facies of the Fucoïd Marls (Central Italy). *Geobios* 11, 225-236.
- 1161 Raddadi, M.C., 2004. Etude de la nature de la radioactivité gamma dans les roches carbonatées de plate-forme :
1162 analyses et interprétations environnementales, diagénétiques et géodynamiques. *Géologie Alpine, Mémoire*
1163 *hors série* 45, 168 pp.
- 1164 Reboulet, S., et alli. 2018. Report on the 6th International Meeting of the IUGS Lower Cretaceous Ammonite
1165 Working Group, the Kilian Group (Vienna, Austria, 20th August 2017). *Cretaceous Research* 91, 100-110.
- 1166 Rey, J., Canérot, J., Peybernès, B., Taj-Eddine, K., Rahhali, I., Thieuloy, J-P. 1986. Le Crétacé inférieur de la
1167 région d'Essaouira : données biostratigraphiques et évolutions sédimentaires. *PICG – UNESCO section*
1168 *Sciences de la Terre* 183, *Revue de la Faculté des sciences de Marrakech, numéro spécial* 2, 413-441.

- 1169 Rey, J., Canérot, J., Peybernès, B., Taj-Eddine, K., Thieuloy, J.-P., 1988. Lithostratigraphy, biostratigraphy and
1170 sedimentary dynamics of the Lower Cretaceous deposits on the northern side of the western High Atlas
1171 (Morocco). *Cretaceous Research* 9, 141-158.
- 1172 Roch, E., 1930. Histoire stratigraphique du Maroc. Notes et Mémoires du Service géologique du Maroc 80, 440
1173 pp.
- 1174 Roth, P.H., 1981. Mid-Cretaceous calcareous nannoplankton from the Central Pacific: implications for
1175 paleoceanography. In: Thiede, J. et al. (Eds.): Initial Reports of the Deep Sea Drilling Project 62, 471-489.
- 1176 Roth, P.H., 1983. Jurassic and Lower Cretaceous calcareous nannofossils in the western North Atlantic (Site 534):
1177 biostratigraphy, preservation, and some observations on biogeography and paleoceanography. In: Sheridan
1178 R.E., Gradstein F.M., et al. (Eds.), Initial Reports of the Deep Sea Drilling Project 76. U.S. Government
1179 Printing Office, Washington, 587-621.
- 1180 Roth, P.H., 1989. Ocean circulation and calcareous nannoplankton evolution during the Jurassic and Cretaceous.
1181 *Palaeogeography, Palaeoclimatology, Palaeoecology* 74, 111-126.
- 1182 Roth, P.H., Bowdler, J., 1981. Middle Cretaceous nannoplankton biogeography and oceanography of the Atlantic
1183 Ocean. In: Warme J.E., Douglas R.G., Winterer E.L., (Eds), *The Deep Sea Drilling Project: a Decade of*
1184 *Progress. SEPM. Sp. Publ. 32*, 517-546.
- 1185 Roth, P.H., Krumbach, K.P., 1986. Middle Cretaceous calcareous nannofossil biogeography and preservation in
1186 the Atlantic and Indian Oceans: Implications for paleoceanography. *Marine Micropaleontology* 10, 235-266.
- 1187 Ruiz-Ortiz, P.A., Castro, J.M., 1998. Depositional sequences in shallow to hemipelagic platform deposits; Aptian,
1188 Prebetic, Alicante (SE Spain). *Bulletin de la Société géologique de France* 169, 21-33.
- 1189 Sabatino, N., Coccioni, R., Manta, D.S., Baudin, F., Vallefucio, M., Traina, A., Sprovieri, M., 2015. High-
1190 resolution chemostratigraphy of the late Aptian–early Albian oceanic anoxic event (OAE 1b) from the Poggio
1191 le Guaine section (Umbria–Marche Basin, central Italy). *Palaeogeography, Palaeoclimatology, Palaeoecology*
1192 426, 319-333.
- 1193 Scarparo Cunha, A.A., Shimabukuro, I., 1997. Braarudosphaera blooms and anomalous enrichment of
1194 Nannoconus: evidence from Turonian South Atlantic, Santos Basin, Brazil. *Journal of Nannoplankton*
1195 *Research* 19, 51-55.
- 1196 Schettino, A., Turco, E., 2009. Breakup of Pangaea and plate kinematics of the central Atlantic and Atlas regions.
1197 *Geophysical Journal International* 178, 1078-1097.
- 1198 Schlager, W., 2003. Benthic carbonate factories of the Phanerozoic. *International Journal of Earth Sciences* 92,
1199 445-464.
- 1200 Schlanger, S.O., Jenkyns, H.C., 1976. Oceanic anoxic events : Causes and consequences. *Geologie en Mijnbouw*
1201 55, 179-184.
- 1202 Skelton, P.W., Gili, E., 2012. Rudists and carbonate platforms in the Aptian: a case study on biotic interactions
1203 with ocean chemistry and climate. *Sedimentology* 59, 81–117.
- 1204 Stets, J., 1992. Mid-Jurassic events in the Western High Atlas (Morocco). *Geologische Rundschau* 81, 68-84.
- 1205 Stewart, S.A., 2006. Implications of passive salt diaper kinematics for reservoir szgmzntation by radial and
1206 concentric faults. *Marine and Petroleum Geology*, 23, 843-853.
- 1207 Street, C., Bown, P.R., 2000. Palaeobiogeography of early Cretaceous (Berriasian-Barremian) calcareous
1208 nannoplankton. *Marine Micropaleontology* 39, 265-291.
- 1209 Tappan, H.L., 1980. The paleobiology of plant protists. San Francisco, 1028 p.
- 1210 Tari, G., Jabour, H., 2013. Salt tectonics along the Atlantic margin of Morocco. Geological Society, London,
1211 Special Publications 369, 337-353.
- 1212 Tendil, A.J.-B., Frau, C., Léonide, P., Fournier, F., Borgomano, J.R., Lanteaume, C., Masse, J.-P., Masonnat, G.,
1213 Rolando, J.-P., 2018. Plateforme-to-basin anatomy of a Barremian-Aptian Tethyan carbonate system: New
1214 insights into regional factors controlling the stratigraphic architecture of the Urgonian Provence platform
1215 (southeast France). *Cretaceous Research* 91, 382-411.
- 1216 Trabucho-Alexandre, J., von Gilst, R.I., Rodríguez-López, J.P., de Boer, P.L., 2011. The sedimentary expression
1217 of oceanic anoxic event 1b in the North Atlantic. *Sedimentology* 58, 1217-1246.
- 1218 Tucker, M.E., Wright, V.P., 1990. Carbonate sedimentology, Blackwell, Oxford, 496 pp.
- 1219 Vila, J.-M., 1980. *La chaîne alpine d'Algérie orientale et des confins algéro-tunisiens*. Thèse Doctorat ès Sciences,
1220 Univ. Pierre et Marie Curie, Paris VI, 665 pp., 40 pl., 3 vol.
- 1221 Watkins, D.K., 1989. Nannoplankton productivity fluctuations and rhythmically-bedded pelagic carbonates of the
1222 Greenhorn Limestone (Upper Cretaceous). *Palaeogeography, Palaeoclimatology, Palaeoecology* 74, 75-86.
- 1223 Watkins, D.K., Wise, S.W., Pospichal, J.J., Crux, J., 1996. Upper Cretaceous calcareous nannofossil
1224 biostratigraphy and paleoceanography of the Southern Ocean. In: Moguevski A., Whatley R. (eds):
1225 *Microfossils and Oceanic Environments*, University of Wales, Aberystwyth Press, 355-381.
- 1226 Wiedmann, J., Butt, A., Einsele, G., 1978. Vergleich von marokkanischen Kreide-Küstenaufschlüssen und
1227 Tiefseebohrungen (DSDP): Stratigraphie, Paläonenvironment und Subsidenz an einem passive
1228 Kontinentalrand. *Geologische Rundschau* 67, 454-508.

- 1229 Wiedmann, J., Butt, A., Einsele, G., 1982. Cretaceous Stratigraphy, Environment, and Subsidence History at the
1230 Moroccan Continental Margin. In: von Rad, U. et al (Eds.), *Geology of the Northwest African Continental*
1231 *Margin*, 366-395, Springer-Verlag.
- 1232 Williams, J.R., Bralower, T.J., 1995. Nannofossil assemblages, fine fraction isotopes, and the paleoceanography
1233 of the Valanginian-Barremian (Early Cretaceous) North Sea Basin. *Paleoceanography* 10, 815-839.
- 1234 Wise, S.W., 1988. Mesozoic-Cenozoic history of calcareous nannofossils in the region of the Southern Ocean.
1235 *Palaeogeography, Palaeoclimatology, Palaeoecology* 67, 157-179.
- 1236 Witam, O., 1998. Le Barrémien-Aptien de l'Atlas Occidental (Maroc) : lithostratigraphie, biostratigraphie,
1237 sédimentologie, stratigraphie séquentielle, géodynamique et paléontologie. *Strata* 30, 1-421.
- 1238 Zühlke, R., Bouaouda, M.-S., Ouajhain, B., Bechstadt, T., Leinfelder, R., 2004. Quantitative Meso/Cenozoic
1239 development of the eastern Central Atlantic continental Shelf, western High Atlas, Morocco. *Marine and*
1240 *Petroleum*